Annual Methodological Archive Research Review
http://amresearchreview.com/index.php/Journal/about
Volume 4, Issue 2(2026)

Online ISSN 3007-3197
Print ISSN 3007-3189

http://amresearchreview.com/index.php/Journal/about

Synthesis and Characterization of Hexaferrite Materials for Advanced Magnetic Applications

Ghulam Abbas
Department of Physics, University of Southern Punjab Multan
Email: abbas9017544@gmail.com

Muhammad Mudassir
Institute of Physics, The Islamic University of Bahawalpur, Bahawalpur, Pakistan
Email: mmudassar168@gmail.com

Shah Wali Ullah
Ph.D. Student, Advanced Functional Materials (AFM) Laboratory, Engineering Physics Department, Institute of Technology Bandung, Bandung 40132, Indonesia
Email: 33323751@mahasiswa.itb.ac.id

Ghufran ur Rehman
Pak-Austria Fachhochschule: Institute of Applied Sciences and Technology
Haripur, Pakistan Email: ghufran_rehman@live.com

ABSTRACT

Hexagonal ferrites (hexaferrites) are iron-based oxides that combine strong magnetocrystalline anisotropy, high electrical resistivity, chemical stability and low cost. They supply most of the world's permanent magnets by mass and are central to microwave, recording and magnetoelectric devices. Their performance depends more on how they are made than on their nominal composition, because synthesis controls phase purity, cation distribution and particle size, and each of these sets the coercivity and magnetisation that a device can use. In this research article we combine crystallographic simulation, analytical magnetic modelling and a quantitative analysis of reported synthesis–property data. First, we reconstructed the structure of $BaFe_{12}O_{19}$ and $SrFe_{12}O_{19}$ from published crystallographic data and computed their powder X-ray diffraction fingerprints, X-ray densities (5.30 and 5.11 g cm^{-3}) and sublattice moments (20 μ_B per formula unit, equivalent to 100.5 and 105.2 emu g^{-1} at 0 K). From the room-temperature anisotropy constants we derived anisotropy fields of 17.3 and 18.5 kOe, Stoner–Wohlfarth coercivity limits of 8.3 and 8.9 kOe, a single-domain critical diameter of about 0.55 µm and a superparamagnetic threshold near 8 nm. Second, we compiled reported data on synthesis temperature, saturation magnetisation (M_s) and coercivity (H_c) across routes and substitutions. Chemical routes lower the formation temperature from above 900 °C to as little as 150 °C. Aluminium substitution trades magnetisation for coercivity: in $SrFe_{12-x}Al_xO_{19}$, M_s falls from 47.5 to 12.9 emu g^{-1} while H_c rises from 9.1 to 18.5 kOe as x increases from 1.5 to 4. Calcium co-substitution raises H_c to 21.3 kOe and, at higher aluminium content, to 36 kOe, while the Curie

Annual Methodological Archive Research Review
http://amresearchreview.com/index.php/Journal/about
Volume 4, Issue 2(2026)

Online ISSN 3007-3197
Print ISSN 3007-3189
http://amresearchreview.com/index.php/Journal/about

temperature falls by about 60 K per unit of x. A property map places the reported materials in three application regimes: soft planar ferrites for gigahertz inductors and antennas, M-type magnets and microwave components, and ultra-hard substituted phases for millimetre-wave absorbers. We close with a reporting checklist covering phase quantification, unit consistency and particle-size control, and with the research directions that the compiled evidence supports.

Keywords: Hexaferrite; Barium Ferrite; Strontium Ferrite; Sol–Gel Auto-Combustion; Magnetocrystalline Anisotropy; Coercivity; X-Ray Diffraction; Permanent Magnets; Microwave Absorbers; Magnetoelectric Materials

Introduction

Background and motivation

The hexagonal ferrites were introduced by Philips in the early 1950s as Ferroxdure, a family of oxide permanent magnets that needed neither cobalt nor nickel [1]. Their crystal chemistry was resolved soon after, when Braun showed that the different members of the family are built by stacking a small number of spinel and barium-containing blocks along the hexagonal *c* axis [2]. The classic monograph of Smit and Wijn then set out the magnetic data that are still quoted today [3]. Seventy years later the M-type compounds $BaFe_{12}O_{19}$ (BaM) and $SrFe_{12}O_{19}$ (SrM) remain the most widely produced magnetic materials by mass, mainly because the raw materials are abundant and the products resist corrosion and oxidation [4–6].

Interest in the family has grown well beyond permanent magnets. The large uniaxial anisotropy field of M-type ferrites, together with their high resistivity, makes them useful as self-biased materials for circulators, isolators and filters at microwave and millimetre-wave frequencies [7–9]. Barium ferrite particles have been used in perpendicular and tape recording for four decades [10, 11]. Several Y-, Z- and M-type compounds show magnetoelectric coupling driven by helical or conical spin order, and some do so at room temperature [12–15]. More recently, heavily substituted M-type phases have reached coercivities above 20 kOe and natural ferromagnetic resonance frequencies in the sub-terahertz range [16, 17].

Figure 1 summarises the main milestones. The first three decades established the structures, intrinsic properties and processing of the hard M-type magnets [1–3, 18]. Recording media and microwave devices followed [8, 10], and since 2000 the field has diversified into rare-earth-reduced high-grade magnets, magnetoelectric phases, low-temperature nanoparticle synthesis and, most recently, ultra-hard substituted ferrites for the sub-terahertz range [11–13, 16, 17, 19–21].

Annual Methodological Archive Research Review
http://amresearchreview.com/index.php/Journal/about
Volume 4, Issue 2(2026)

Online ISSN 3007-3197
Print ISSN 3007-3189
http://amresearchreview.com/index.php/Journal/about

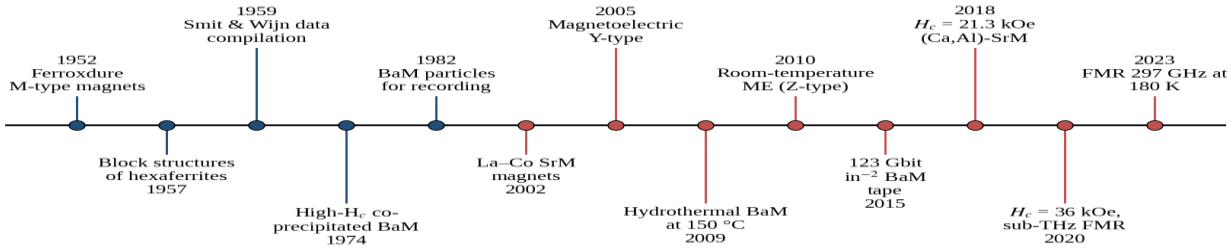


Figure 1. Selected milestones in hexaferrite research, compiled from [1–3, 10–13, 16–21].

Problem statement

The intrinsic properties of a hexaferrite are fixed by its crystal structure and composition, but the properties that reach a device are extrinsic. Coercivity depends on particle size and shape, on the presence of secondary phases such as α-Fe_2O_3, and on where substituent cations sit in the lattice [4, 22]. These features are set during synthesis. The same nominal composition can therefore give coercivities that differ by an order of magnitude when it is prepared by different routes or calcined at different temperatures [16, 18, 23]. A researcher who wants a particular combination of magnetisation, coercivity and operating frequency has to choose among many synthesis routes and dopant schemes, and the published results are reported in mixed units and are rarely compared on a common basis.

Research gap

Broad reviews describe the structures, synthesis routes and applications of the family in depth [4, 7, 8], and recent reviews focus on permanent magnets [6] or on giant coercivity [24]. Three gaps remain. First, few reviews connect the reported extrinsic values to quantitative intrinsic limits, such as the anisotropy field, the Stoner–Wohlfarth coercivity and the single-domain size, computed in one consistent framework. Second, characterisation is often reported without a reference diffraction fingerprint or with unit conversions that are not stated, which makes cross-study comparison unreliable. Third, recent results on aluminium and calcium–aluminium substituted SrM, which change the property space available to ferrites, have not been placed alongside classical M, X and U data on a single map linked to applications.

Objectives and research questions

This study has four objectives: (i) to summarise the crystal chemistry and the origin of magnetism in hexaferrites in a form that can be used directly to interpret measurements; (ii) to compare the main synthesis routes by their formation temperature and their effect on phase purity and particle size; (iii) to compute reference diffraction and magnetic parameters for BaM and SrM and compare them with reported data; and (iv) to compile reported magnetic data into a property map that links synthesis and substitution to applications. We address three questions. RQ1: how far below the intrinsic limits do synthesised hexaferrites operate, and why? RQ2: which synthesis and substitution

Annual Methodological Archive Research Review
http://amresearchreview.com/index.php/Journal/about
Volume 4, Issue 2(2026)

Online ISSN 3007-3197
Print ISSN 3007-3189
http://amresearchreview.com/index.php/Journal/about

strategies move a material most effectively along the trade-off between magnetisation and coercivity? RQ3: what reporting practice would make results across studies comparable?

Scope and organisation

The study covers the M, W, X, Y, Z and U families, with most attention on the M-type compounds because they dominate both production and the quantitative literature [4, 6]. Spinel and garnet ferrites are discussed only where they serve as a comparison. Section 2 surveys crystal chemistry, magnetism, synthesis, substitution, characterisation, soft and magnetoelectric phases, films and composites, and applications. Section 3 describes how the literature was selected and how the reference parameters were computed. Section 4 presents the computed structural and magnetic references and the compiled data on synthesis, substitution, resonance frequency and energy product. Section 5 discusses the findings against the research questions and sets out practical recommendations, and Section 6 concludes.

Literature Review

Crystal chemistry and classification

All hexaferrites can be placed in the ternary system $BaO–MeO–Fe_2O_3$, where Me is a small divalent cation such as Co, Zn, Ni, Mg or Fe (Figure 2). The M phase, $BaO·6Fe_2O_3$, lies on the $BaO–Fe_2O_3$ edge. The W phase is obtained by adding two spinel units to M, the Y phase lies at $2BaO·2MeO·6Fe_2O_3$, and the Z and U phases lie on the line joining M and Y, being M + Y and 2M + Y respectively [3, 4]. The X phase, 2M + 2S, lies on the M–S line together with W. This geometry is useful in practice, because a composition that drifts during processing will move towards the phases on the nearest tie line, and these are the impurities most likely to appear in a diffraction pattern.

Annual Methodological Archive Research Review
http://amresearchreview.com/index.php/Journal/about
Volume 4, Issue 2(2026)

Online ISSN 3007-3197
Print ISSN 3007-3189

http://amresearchreview.com/index.php/Journal/about

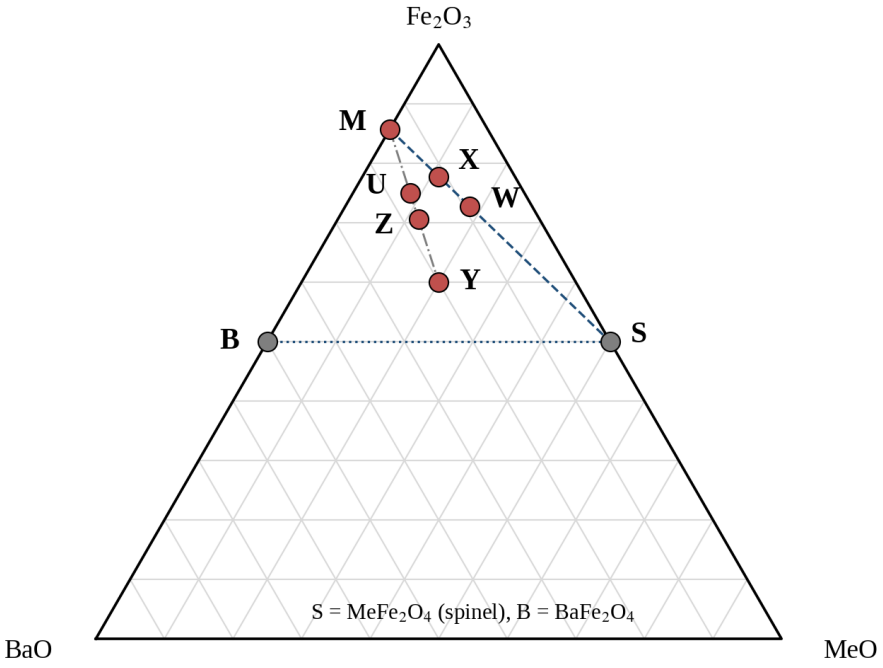


Figure 2. Compositions of the hexaferrite phases in the BaO–MeO–Fe_2O_3 system, plotted from their stoichiometry [3, 4]. W and X lie on the M–S tie line (dashed), Z and U lie on the M–Y line (dash-dot), and B–S (dotted) joins $BaFe_2O_4$ and the spinel $MeFe_2O_4$.

Structurally, the phases are stacks of three block types. The S block is a two-layer spinel slab of composition $Me_2Fe_4O_8$ or Fe_6O_8; the R block is a three-layer hexagonal slab containing one Ba ion, $(BaFe_6O_{11})^{2-}$; and the T block is a four-layer slab containing two Ba ions [2, 4]. The M phase is RSR*S*, where the asterisk denotes rotation by 180° about *c*, giving a hexagonal cell in space group $P6_3/mmc$ with $a \approx 5.89$ Å, $c \approx 23.2$ Å and two formula units per cell [25, 26]. The other phases have longer stacking sequences and correspondingly longer *c* axes, from about 32.8 Å for W to about 113 Å for U (Table 1). The long periods and close structural similarity of the phases explain why intergrowths and stacking faults are common and why the pure X and U phases are difficult to prepare [4, 27].

Table 1. Structural and magnetic characteristics of the main hexaferrite types. Room-temperature M_s and T_C are representative values from the compilations in [3, 4] unless noted.

Type	Formula (example)	Block stacking	c (Å)	Character	M_s (emu g^{-1}); T_C (°C)
M	$BaFe_{12}O_{19}$	RSR*S*	23.2	Hard, uniaxial	72; 450
W	$BaMe_2Fe_{16}O_{27}$ (Fe_2W)	RSSR*S*S*	32.8	Uniaxial or cone/plane (Co)	78; 455
Y	$Ba_2Me_2Fe_{12}O_{22}$ (Co_2Y, Zn_2Y)	$(TS)_3$	43.6	Soft, easy plane	34; 340 (Co_2Y); 42; 130 (Zn_2Y)

Annual Methodological Archive Research Review
http://amresearchreview.com/index.php/Journal/about
Volume 4, Issue 2(2026)

Online ISSN 3007-3197
Print ISSN 3007-3189
http://amresearchreview.com/index.php/Journal/about

Type	Formula (example)	Block stacking	c (Å)	Character	M_s (emu g^{-1}); T_C (°C)
Z	$Ba_3Me_2Fe_{24}O_{41}$ (Co_2Z)	RSTSR*S*T*S*	52.3	Soft, easy plane	50; 410
X	$Ba_2Me_2Fe_{28}O_{46}$ (Co_2X)	$(RSR*S*S*)_3$	84.1	Intermediate	45.0 (sol–gel fibres) [27]
U	$Ba_4Me_2Fe_{36}O_{60}$ (Co_2U)	RSR*S*T*S*	113.1	Soft	51.5 (sol–gel fibres) [27]

Me denotes a divalent cation. Values for X and U refer to sol–gel fibres because single-phase bulk data are scarce. Asterisks in stacking sequences denote blocks rotated by 180° about the c axis.

Origin of magnetisation and anisotropy

In the M structure the Fe^{3+} ions occupy five crystallographic sites: three octahedral sites (12k, 2a and $4f_2$), one tetrahedral site ($4f_1$) and one five-fold trigonal-bipyramidal site (2b) inside the R block [22, 25]. Superexchange through oxygen aligns the 12k, 2a and 2b moments in one direction and the $4f_1$ and $4f_2$ moments in the other, in the collinear Gorter model [3] (Figure 3). With 5 μ_B per Fe^{3+} ion this gives a net moment of 20 μ_B per formula unit at 0 K, which is close to the measured low-temperature value and is the basis of all site-substitution arguments [22, 28]. Mössbauer spectroscopy resolves the five sites by their hyperfine fields and is the most direct way to see where a substituent goes [29, 30].

The strong uniaxial anisotropy of M-type ferrites, with $K_1 \approx 3.3 \times 10^6$ erg cm^{-3} for BaM at room temperature [28], arises mainly from the 2b site, where the trigonal-bipyramidal coordination produces a large single-ion contribution, with smaller contributions from the $4f_1$ and 12k sites [22]. This is why substitutions on 2b and 12k change H_c so strongly. In the Co-containing Y and Z phases, by contrast, Co^{2+} in octahedral sites favours an easy plane, which gives high initial permeability up to frequencies far above those of spinel ferrites and suits inductors and antennas [3, 4].

Annual Methodological Archive Research Review
http://amresearchreview.com/index.php/Journal/about
Volume 4, Issue 2(2026)

Online ISSN 3007-3197
Print ISSN 3007-3189
http://amresearchreview.com/index.php/Journal/about

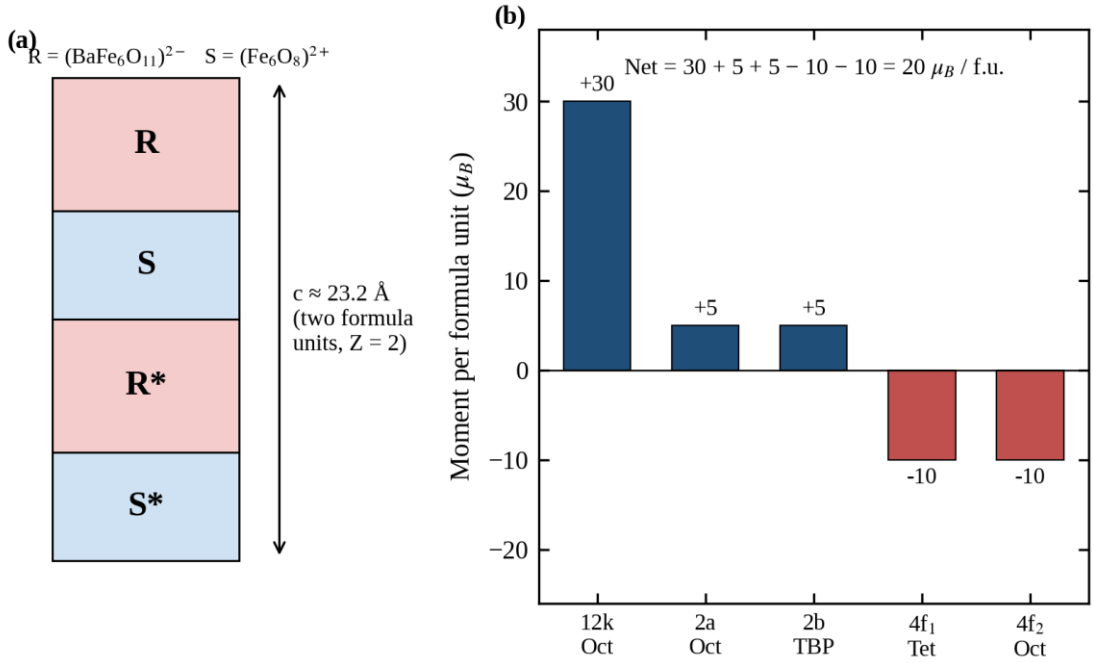


Figure 3. (a) Block stacking of the M-type unit cell (RSR*S*); the asterisk denotes rotation by 180° about the c axis [2, 25]. (b) Fe^{3+} sublattice moments per formula unit in the Gorter model (5 μ_B per ion; spin-up positive), computed in this work. Oct, octahedral; Tet, tetrahedral; TBP, trigonal bipyramidal.

Synthesis routes

The industrial route is the ceramic method: $BaCO_3$ or $SrCO_3$ and Fe_2O_3 are mixed, calcined, milled to about 1 μm, pressed in a magnetic field and sintered [4, 6]. It is cheap and scalable but needs high temperatures, and milling introduces strain and defects that lower coercivity [18]. Chemical routes were developed to reach smaller and more uniform particles at lower temperatures. Haneda and co-workers heated a filtered $BaCO_3/Fe(OH)_3$ co-precipitate at 925 °C and obtained BaM with coercivity close to the single-domain value, which showed early that powder quality, rather than composition, limited H_c [18]. Glass crystallisation [31], molten-salt synthesis [32] and mechanical alloying [33] followed, each trading process complexity for control of particle size or shape.

Sol–gel and auto-combustion methods are now the most common laboratory routes (Figure 4a). Metal nitrates are complexed with citric acid or another chelating agent, the gel is dried and ignited, and the resulting precursor is calcined, typically between 900 and 1200 °C [16, 23, 34]. The approach descends from the Pechini process [35]. It gives mixing at the molecular level, which is especially important for highly substituted compositions where poorly reactive cations such as Al^{3+} otherwise segregate [16, 36]. Hydrothermal synthesis reaches the lowest temperatures: in a large excess of hydroxide, BaM forms at temperatures as low as 150 °C and, with oleic acid, uniform ultrafine particles can be grown at up to 240 °C [20]. These particles are discs about 10 nm wide and 3 nm thick, close to the cell height along *c*, and are superparamagnetic [37, 38].

Annual Methodological Archive Research Review
http://amresearchreview.com/index.php/Journal/about
Volume 4, Issue 2(2026)

Online ISSN 3007-3197
Print ISSN 3007-3189
http://amresearchreview.com/index.php/Journal/about

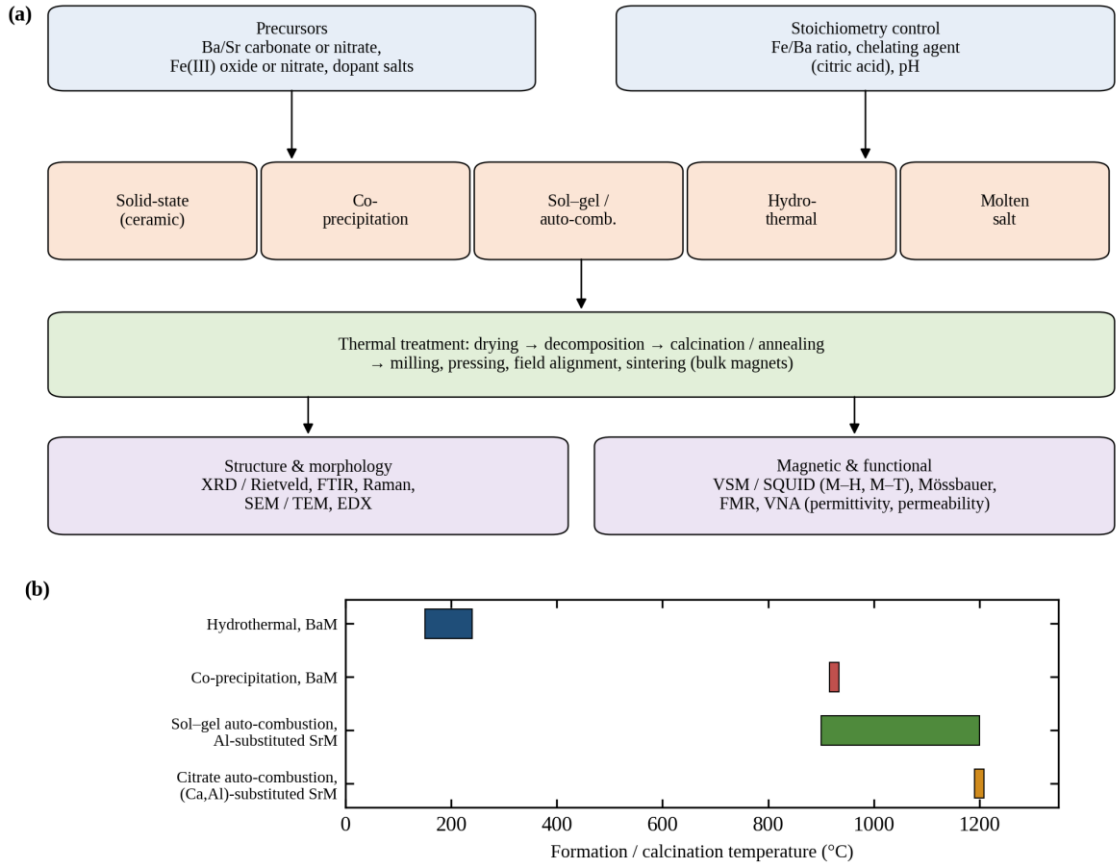


Figure 4. (a) General workflow for the synthesis and characterisation of hexaferrites, summarised from the reviewed studies [4, 8]. (b) Reported formation or calcination temperatures for four routes: hydrothermal BaM [20], co-precipitated BaM [18], sol–gel auto-combustion Al-substituted SrM [23] and citrate auto-combustion (Ca,Al)-substituted SrM [16].

The chemistry of phase formation explains much of this behaviour. In the $BaO–Fe_2O_3$ system, $BaFe_{12}O_{19}$ is the stable iron-rich compound, but it rarely forms directly from the oxides [4]. On heating a carbonate–oxide mixture, $BaCO_3$ first reacts with part of the Fe_2O_3 to give the spinel-related $BaFe_2O_4$, which then reacts with the remaining hematite to form the M phase; residual α-Fe_2O_3 and $BaFe_2O_4$ are therefore the usual impurities of incomplete reaction [4, 22]. Because Ba and Sr are partly lost or segregated during processing, many studies use a slightly Fe-deficient nominal ratio (Fe/Ba below 12) to suppress hematite [4]. In wet-chemical routes the intermediate steps are different. Precursors decompose to an amorphous or poorly crystalline oxide in which the cations are already mixed, and the M phase can then crystallise with little long-range diffusion, which is why co-precipitated and sol–gel powders form the M phase several hundred degrees below the ceramic route [18, 23]. In sol–gel fibres, retained halide stabilised the intermediate oxides and delayed M-phase formation until the halide was lost [39].

After synthesis, bulk magnets require densification and texture. Industrial anisotropic magnets are made by wet pressing a slurry of fine single-domain particles in a magnetic

Annual Methodological Archive Research Review
http://amresearchreview.com/index.php/Journal/about
Volume 4, Issue 2(2026)

Online ISSN 3007-3197
Print ISSN 3007-3189
http://amresearchreview.com/index.php/Journal/about

field, which aligns the platelets with their c axes parallel, followed by sintering [6, 19]. The conflict is that sintering promotes grain growth above the single-domain size, which lowers H_c, while insufficient densification lowers remanence. Small additions such as SiO_2 and CaO, applied in commercial practice, segregate to grain boundaries and limit grain growth [6, 19]. Field-assisted and pressure-assisted sintering, as well as the alignment of single-domain particles in polymer binders, have been used to obtain dense or textured bodies without losing coercivity [6, 17].

Cation substitution

Substitution is the second main lever after synthesis. La–Co co-substitution in SrM, in which La^{3+} replaces Sr^{2+} and Co^{2+} replaces Fe^{3+}, raised the anisotropy and became the basis of the highest-grade commercial ferrite magnets [19]. Mössbauer and Raman studies placed most Co^{2+} on the $4f_2$ and 2a sites and showed a partial $Fe^{3+}\rightarrow Fe^{2+}$ change on 2a [30, 40], and the anisotropy of these compositions was later analysed in terms of higher-order constants [41]. Diamagnetic Al^{3+} works differently. It lowers M_s by diluting the magnetic sublattices but, in single-domain particles, raises H_c because the anisotropy field increases faster than the magnetisation falls [23, 34]. Trusov *et al.* showed that co-substituting Ca for Sr increases the effect, reaching 21.3 kOe at x = 4 [16], and Gorbachev *et al.* extended the series to 36 kOe at x = 5.5 [17]. Neutron diffraction places Al first on the 2a and 12k sites and on the 4e and 4f sites at higher contents, and shows that Al enters the lattice effectively only in the sol–gel route [36].

Characterisation practice

Most studies combine X-ray diffraction with Rietveld refinement [42] to identify phases and refine lattice parameters, a line-broadening analysis by the Scherrer or Williamson–Hall method [43, 44] to estimate crystallite size, infrared and Raman spectroscopy to confirm metal–oxygen bonding [45, 46], electron microscopy for morphology, and vibrating-sample or SQUID magnetometry for hysteresis loops. Mössbauer spectroscopy and neutron diffraction are less common but are the only methods that resolve site occupancy directly [29, 36]. Microwave work adds ferromagnetic resonance and vector-network-analyser measurements of complex permittivity and permeability [7, 47]. Table 2 summarises what each technique provides and where it is most often misused. The weak points in practice are well known: small amounts of α-Fe_2O_3 are easily missed and lower M_s; crystallite size from line broadening is often reported as particle size; and M_s is quoted at fields that do not saturate highly anisotropic samples [4, 16].

Table 2. Characterisation techniques used for hexaferrites, the information they provide

Annual Methodological Archive Research Review
http://amresearchreview.com/index.php/Journal/about
Volume 4, Issue 2(2026)

Online ISSN 3007-3197
Print ISSN 3007-3189
http://amresearchreview.com/index.php/Journal/about

and common pitfalls.

Technique	Information obtained	Hexaferrite-specific signature	Common pitfall
XRD with Rietveld refinement [42]	Phase identity and fractions, lattice parameters, site occupancy (approximate)	(114) and (107) as strongest M-type reflections; (00l) and (2 0 11) sensitive to c	Weak α-Fe_2O_3 or $BaFe_2O_4$ peaks missed; preferred orientation of platelets
Line-broadening analysis [43, 44]	Coherent crystallite size and microstrain	Anisotropic broadening of (00l) versus (hk0) in platelets	Crystallite size reported as particle size
FTIR [45]	Metal–oxygen stretching, residual organics and nitrates	Bands below about 600 cm^{-1} from Fe–O in octahedral and tetrahedral sites	Cannot separate hexaferrite from spinel or hematite by itself
Raman [46]	Local symmetry and site-specific vibrations	Modes assigned to 12k, 2b and $4f_1$/$4f_2$ environments	Laser heating can transform the surface
SEM / TEM with EDX	Particle size, shape, aspect ratio, composition	Hexagonal platelets with c normal to the plate	Agglomerates counted as particles
VSM / SQUID	M_s, M_r, H_c, loop shape, T_C from M(T)	$M_r/M_s \approx 0.5$ for random single-domain assemblies [48]	Fields too low to saturate; unit errors
Mössbauer [29, 30]	Fe site occupancy, valence, hyperfine fields	Five Fe sextets (12k, 2a, 2b, $4f_1$, $4f_2$)	Overlapping sextets require constrained fits
Neutron diffraction [36]	Site occupancy of light or similar-Z ions; magnetic structure	Distinguishes Al from Fe on 2a, 12k, 4e and 4f	Limited access; large sample mass
FMR / VNA [7, 9]	Resonance frequency, linewidth, ε and μ spectra	Natural resonance set by H_A	Sample-shape demagnetising effects ignored

Soft and planar hexaferrites

The Y-, Z- and U-type compounds containing Co are magnetically soft because their easy direction lies in, or close to, the basal plane [3, 4]. In such materials the magnetisation can rotate easily within the plane but is held strongly against rotation out of it. The result is a high permeability that persists to much higher frequencies than in cubic spinel ferrites, which are limited by Snoek's relation between permeability and resonance frequency [3]. This is why Co_2Z and Co_2Y were developed for inductors and antenna substrates in the hundreds of megahertz to low gigahertz range [4, 9]. Their main processing difficulty is phase purity. The formation windows of Y, Z and U are narrow, Z decomposes into M and Y at high temperature, and intergrowths are common, so most reports describe mixtures rather than single phases [4, 27]. Sol–gel processing improves homogeneity; aligned Co_2X and Co_2U fibres formed at 1200 °C

Annual Methodological Archive Research Review
http://amresearchreview.com/index.php/Journal/about
Volume 4, Issue 2(2026)

Online ISSN 3007-3197
Print ISSN 3007-3189
http://amresearchreview.com/index.php/Journal/about

with M_s of 45.0 and 51.5 emu g^{-1} and coercivities of 0.085 and 0.059 T, respectively [27].

Magnetoelectric hexaferrites

In some hexaferrites the competition between exchange interactions in the L and S blocks produces helical or conical spin order. A transverse conical structure breaks inversion symmetry and induces an electric polarisation through the spin-current mechanism, so a magnetic field can switch or rotate the polarisation [15]. The effect was first reported in a Zn_2Y-type compound [12], and in $Ba_2Mg_2Fe_{12}O_{22}$ a field of about 30 mT was enough to control the polarisation vector [49]. The decisive step towards applications came with Z-type $Sr_3Co_2Fe_{24}O_{41}$, which showed a low-field magnetoelectric effect at room temperature [13]. A $Ba_{0.52}Sr_{2.48}Co_2Fe_{24}O_{41}$ single crystal then demonstrated electric-field control of four non-volatile magnetisation states at room temperature [50], and Sc-doped M-type ferrites stabilised conical order to near room temperature with magnetically controllable spin helicity [14]. These materials are insulating, which limits leakage, but their coupling coefficients are small and most experiments still use single crystals [15].

Films, fibres and composites

Integration into planar microwave circuits requires films with the c axis perpendicular to the substrate, so that the anisotropy field acts as a built-in bias. Pulsed-laser deposition, liquid-phase epitaxy and screen printing have all been used to make such BaM films, and the resulting self-biased devices remove the permanent magnet that conventional circulators need [8, 51, 52]. Fibres are a second form: aligned M-type fibres produced from aqueous sols reach magnetisation values comparable to fine powders and can be woven or embedded for absorbers and composites [27, 39]. Composites combine hexaferrites with polymers or with soft magnetic phases. In polymer composites the ferrite provides magnetic loss at its resonance and the matrix adjusts impedance matching [47]; in exchange-coupled hard–soft composites a soft phase raises remanence while the hard phase preserves coercivity, provided that the soft regions are smaller than about twice the domain-wall width of the hard phase [6, 53].

Applications

Permanent magnets remain the largest market: hexaferrites have a much lower energy product than Nd–Fe–B, but their low cost, corrosion resistance and freedom from rare earths keep them in motors, loudspeakers and sensors [5, 6]. At microwave frequencies, the internal anisotropy field of M-type ferrites provides a built-in bias, which allows self-biased circulators that need no external magnet [8, 52]. Absorbers for electromagnetic compatibility and radar use the natural resonance of M-type ferrites, whose frequency scales with the anisotropy field [7, 47]. Recording uses fine BaM platelets, from early perpendicular media to tape with an areal density of 123 Gbit in^{-2} [10, 11]. Finally, magnetoelectric hexaferrites offer the electric control of magnetisation at room temperature, as shown by four-state magnetisation switching in a Co_2Z single crystal [15, 50].

Annual Methodological Archive Research Review
http://amresearchreview.com/index.php/Journal/about
Volume 4, Issue 2(2026)

Online ISSN 3007-3197
Print ISSN 3007-3189

http://amresearchreview.com/index.php/Journal/about

Synthesis of the literature and research gap

Table 3 summarises representative studies and the questions they leave open. The pattern is consistent: work that reached record values did so by controlling particle size and cation distribution through synthesis, while work that reported only composition and calcination temperature is difficult to compare or reproduce. This study responds by providing a common reference frame (Sections 4.1–4.3), a comparison across routes and substitutions (Sections 4.4–4.8), quantitative estimates for microwave and magnet applications (Sections 4.9–4.10) and a reporting checklist (Section 5.6).

Table 3. Representative studies on hexaferrite synthesis and properties and the questions they leave open.

Study	Material and route	Main finding	Open question
Haneda et al. [18]	BaM, co-precipitation, 925 °C	Coercivity near the single-domain value without milling damage	Scalability; particle-size distribution
Primc et al. [20]	BaM, hydrothermal, 150–240 °C	Lowest reported formation temperature; stable ferrofluids	Superparamagnetic size limits use as hard magnets
Pullar et al. [39]	BaM and SrM fibres, sol–gel	Halide-free sol lowers formation temperature by 200 °C	Fibre alignment versus bulk density
Kools et al. [19]	La–Co SrM, ceramic	Higher anisotropy; basis of top commercial grades	Cost and supply of Co and La
Torkian et al. [23]	Al-SrM, sol–gel auto-combustion	H_c up to 9.1 kOe at x = 2	Secondary phases at low calcination temperature
Trusov et al. [16]	(Ca,Al)-SrM, citrate route, 1200 °C	H_c = 21.3 kOe with single-domain particles	Low M_s (about 14 emu g^{-1})
Gorbachev et al. [21]	(Ca,Al)-SrM, 5–300 K	T_C and lattice shrink with x; H_c peaks below room temperature	Thermal stability for devices
Tokunaga et al. [14]	Sc-doped BaM single crystals	Conical spin order and magnetoelectric response near room temperature	Polycrystalline, low-field operation

Methodology

Research design

The study is a computational and data-driven investigation built on two quantitative analyses: crystallographic and magnetic modelling of the M-type structure, and a harmonised analysis of synthesis and property data reported in the literature (Figure 4a summarises the experimental workflow that the reviewed studies follow). We did not run new syntheses. All numerical results are either taken from the cited primary sources or computed from published crystallographic and magnetic constants, and every computed quantity is identified as such. This design lets us compare reported values with physically defined limits without introducing new measurement uncertainty.

Annual Methodological Archive Research Review
http://amresearchreview.com/index.php/Journal/about
Volume 4, Issue 2(2026)

Online ISSN 3007-3197
Print ISSN 3007-3189
http://amresearchreview.com/index.php/Journal/about

Literature identification and selection

Sources were identified through keyword searches of scholarly databases using combinations of the terms hexaferrite, hexagonal ferrite, $BaFe_{12}O_{19}$, $SrFe_{12}O_{19}$, M-type, W-, X-, Y-, Z- and U-type, sol–gel, auto-combustion, co-precipitation, hydrothermal, substitution, coercivity, magnetoelectric and microwave, and from the reference lists of major reviews [4, 6–8, 24]. We included peer-reviewed studies that reported the synthesis route and conditions together with phase identification and at least one quantitative magnetic property, and foundational works that define structures or constants. We gave priority to studies that confirmed phase purity by diffraction and reported particle size by microscopy, and we excluded results that could not be traced to a primary source.

Each primary source was assessed against four criteria before its numbers were used: (i) phase identity confirmed by diffraction with no unassigned reflections; (ii) synthesis conditions reported in enough detail to be repeated; (iii) the measuring field and temperature stated for magnetic data; and (iv) particle size supported by microscopy where size-dependent properties were discussed. Studies that met all four were used for quantitative figures. Studies that met only some were used qualitatively, and this is indicated in the text.

Data extraction and harmonisation

From each primary source we extracted composition, route, formation or calcination temperature, M_s, H_c, particle size and, where reported, T_C and lattice parameters. Units were harmonised to emu g^{-1} for mass magnetisation (1 A m^2 kg^{-1} = 1 emu g^{-1}) and kOe for field (1 kA m^{-1} = 12.566 Oe; $\mu_0 H$ = 1 T corresponds to 10 kOe). Cell volumes were recalculated from reported *a* and *c* as $V = (\sqrt{3}/2)a^2c$, which reproduced the published values to within 0.1 $Å^3$ [21]. Values read only from figures were not used.

Structural simulation

Structures of BaM and SrM were built in space group $P6_3/mmc$ from the Wyckoff positions of the magnetoplumbite structure [25, 26], with lattice parameters a = 5.8920 Å, c = 23.1830 Å (BaM) and a = 5.8836 Å, c = 23.0376 Å (SrM). The trigonal-bipyramidal Fe was placed on the ideal 2b position. Powder patterns for Cu Kα radiation (λ = 1.5418 Å) were computed with the XRD module of pymatgen [54], which includes atomic scattering factors and Lorentz-polarisation corrections. For display, each reflection was given a Lorentzian profile of 0.24° full width at half maximum. X-ray densities were calculated from the cell contents and volume.

Magnetic estimates

The 0 K moment per formula unit was obtained by summing the sublattice moments of the Gorter model with 5 μ_B per Fe^{3+} [3], and converted to mass magnetisation as $\sigma_0 = n\mu_B N_A/M$. Room-temperature volume magnetisation was taken as $M_s = \sigma_s \rho$, using σ_s = 72 and 74 emu g^{-1} [3, 28]. The anisotropy field is $H_A = 2K_1/M_s$, with $K_1 = 3.3 \times 10^6$ and 3.5×10^6 erg cm^{-3} for BaM and SrM [28]. The coercivity of a randomly oriented assembly of non-interacting single-domain particles is $0.48H_A$ [48]. The critical single-

Annual Methodological Archive Research Review
http://amresearchreview.com/index.php/Journal/about
Volume 4, Issue 2(2026)

Online ISSN 3007-3197
Print ISSN 3007-3189
http://amresearchreview.com/index.php/Journal/about

domain diameter was estimated as $D_c = 72\sqrt{(AK_1)}/(\mu_0 M_s^2)$ [53, 55], with an exchange stiffness $A \approx 6$ pJ m^{-1} [53]. The superparamagnetic diameter D_{sp} was taken from the stability criterion $K_1V = 25k_BT$ at 300 K.

Substitution, resonance and energy-product estimates

Three further estimates were made from published data. (i) Diffraction shifts caused by substitution were computed from Bragg's law and the hexagonal relation $1/d^2 = 4(h^2 + hk + k^2)/(3a^2) + l^2/c^2$, using the lattice parameters reported for $Sr_{1-x/12}Ca_{x/12}Fe_{12-x}Al_xO_{19}$ [21] and the SrM reference values above. (ii) Sublattice dilution was modelled by removing 5 μ_B for each Al^{3+} ion placed on a spin-up site (12k, 2a or 2b) and adding 5 μ_B for each ion placed on a spin-down site ($4f_1$ or $4f_2$), and the result was compared with the measured ratio $M_s(x)/M_s(0)$ [16], taking $M_s(0) = 74$ emu g^{-1} [3]. (iii) The natural ferromagnetic resonance frequency of a uniaxial particle without external field was estimated as $f_r = (\gamma/2\pi)H_A$, with $\gamma/2\pi = 2.80$ GHz kOe^{-1}, which neglects demagnetising corrections [7, 9]; the same relation was inverted to obtain the anisotropy field implied by reported resonance frequencies. The upper bound of the energy product of an ideal, fully dense and fully aligned magnet was taken as $(BH)_{max} = J_s^2/4$, with $J_s = 4\pi M_s$ [53].

Implementation

All calculations and figures were produced in Python 3 with pymatgen [54], NumPy and Matplotlib. Literature data were plotted exactly as reported after unit conversion. The scripts are available from the corresponding author on request.

Results

Compositional and structural landscape

Figure 2 shows that the six phases occupy a narrow region near the Fe_2O_3 corner and fall on two tie lines from the M phase. This has a direct consequence for synthesis: an M-type preparation that is deficient in Ba drifts towards α-Fe_2O_3, while one that picks up a divalent cation moves towards W, and Z and U preparations are prone to M and Y impurities [4]. Figure 3a shows the RSR*S* stacking of the M cell and Figure 3b the sublattice balance that gives 20 μ_B per formula unit. Because the 12k sublattice alone contributes +30 μ_B, a diamagnetic ion placed there reduces M_s most strongly, whereas one placed on a spin-down 4f site can increase it, which is the basis of many Zn and Sn co-substitution schemes [22].

Simulated diffraction fingerprints

The computed patterns (Figure 5, Table 4) reproduce the familiar M-type fingerprint. The (114) reflection at $2\theta = 34.14°$ is the strongest for BaM, followed by (107) at 32.22°, with (110), (203), (2 0 11) and (220) all above 40% of the maximum. SrM gives the same sequence shifted to higher angles. The shift is small for in-plane reflections, 0.04° for (110), because *a* differs by only 0.14%, but larger for reflections with a high *l* index, 0.20° for (008) and 0.27° for (2 0 11), because *c* is 0.63% shorter. The (107)–(114) doublet and the (2 0 11) reflection are therefore the most useful for distinguishing Ba from Sr ferrites or following Al substitution, which shrinks both axes [21]. The

Annual Methodological Archive Research Review
http://amresearchreview.com/index.php/Journal/about
Volume 4, Issue 2(2026)

Online ISSN 3007-3197
Print ISSN 3007-3189

http://amresearchreview.com/index.php/Journal/about

computed X-ray densities are 5.296 g cm^{-3} for BaM and 5.106 g cm^{-3} for SrM; they are the reference values against which the relative density of sintered magnets should be stated.

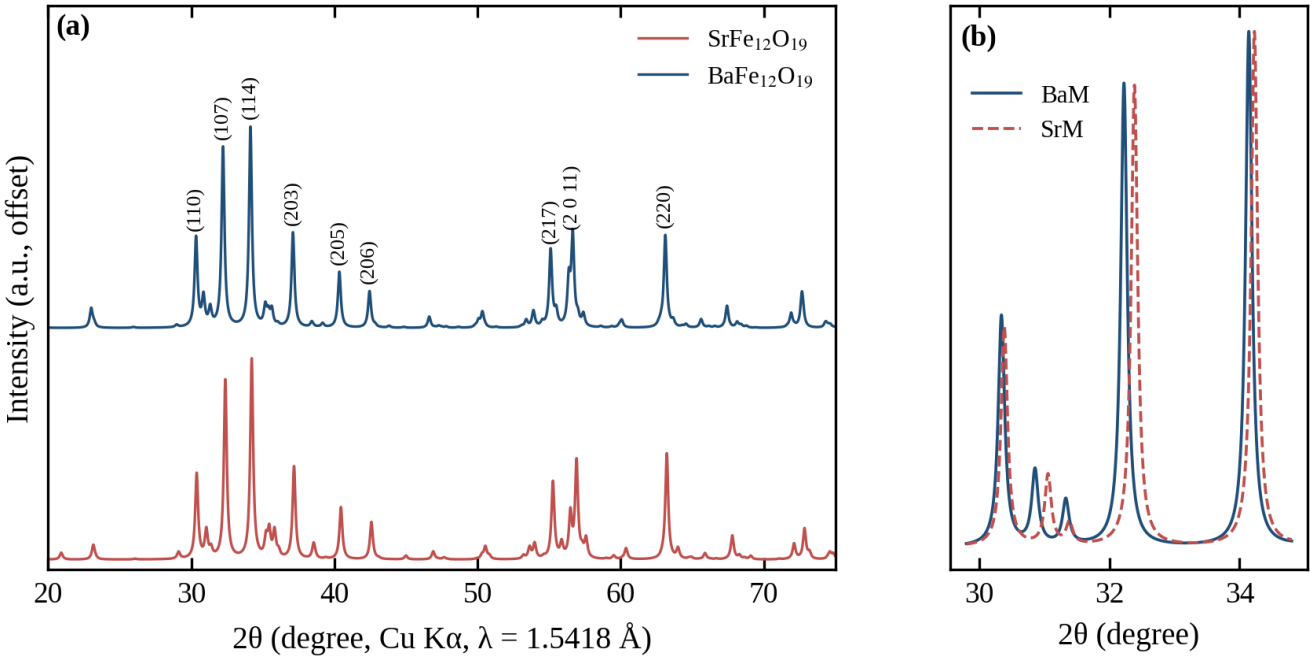


Figure 5. (a) Powder X-ray diffraction patterns of $BaFe_{12}O_{19}$ and $SrFe_{12}O_{19}$ computed in this work from published structural parameters [25, 26] (Cu Kα, Lorentzian FWHM 0.24°). (b) Enlarged 29.8–34.8° region (FWHM 0.12°) showing the shift of the (110), (008), (107) and (114) reflections between the two compounds.

Table 4. Principal computed reflections of $BaFe_{12}O_{19}$ and $SrFe_{12}O_{19}$ (Cu Kα, λ = 1.5418 Å). Intensities are relative to the strongest reflection of each phase.

hkl	2θ BaM (°)	d BaM (Å)	I/I_0 BaM	2θ SrM (°)	d SrM (Å)	I/I_0 SrM
110	30.34	2.946	45	30.38	2.942	43
008	30.86	2.898	14	31.06	2.880	14
107	32.22	2.778	90	32.38	2.765	90
114	34.14	2.626	100	34.23	2.620	100
203	37.11	2.423	47	37.18	2.418	46
205	40.35	2.235	28	40.46	2.230	26
206	42.46	2.129	18	42.59	2.123	19
217	55.11	1.667	38	55.27	1.662	38
2 0 11	56.65	1.625	45	56.92	1.618	48
220	63.12	1.473	46	63.22	1.471	52

Computed in this work with pymatgen [54]; d spacings from Bragg's law.

Annual Methodological Archive Research Review
http://amresearchreview.com/index.php/Journal/about
Volume 4, Issue 2(2026)

Online ISSN 3007-3197
Print ISSN 3007-3189

http://amresearchreview.com/index.php/Journal/about

Intrinsic limits

Table 5 lists the derived parameters. The Gorter model gives 100.5 emu g^{-1} for BaM and 105.2 emu g^{-1} for SrM at 0 K. The room-temperature values of 72 and 74 emu g^{-1} are about 70% of these, consistent with the reduced magnetisation at $T/T_C \approx 0.4$ [28]. The anisotropy fields, 17.3 and 18.5 kOe, imply Stoner–Wohlfarth limits of 8.3 and 8.9 kOe for random assemblies. Some authors quote a lower theoretical maximum of about 7.5 kOe for SrM [23]; the difference reflects the choice of K_1 and M_s, which should therefore always be stated with any such limit. Reported coercivities of unsubstituted M-type powders and fibres are 5–5.5 kOe [39], or 60–65% of the limit. The size thresholds explain why. Figure 6 places $D_{sp} \approx 8$ nm and $D_c \approx 0.55$ µm on a schematic H_c–size curve, which agrees with the critical size of about 500 nm reported for pure SrM [16]. Particles that are too small lose coercivity through thermal activation, as in the superparamagnetic hydrothermal discs [37, 38], while particles above D_c or with surface defects from milling reverse by domain-wall processes at much lower fields [18, 22].

Table 5. Structural and magnetic parameters of $BaFe_{12}O_{19}$ and $SrFe_{12}O_{19}$ derived in this work.

Parameter	BaM	SrM	Basis
Formula units per cell, Z	2	2	$P6_3/mmc$ [25, 26]
Cell volume (Å^3)	697.0	690.6	$V = (\sqrt{3}/2)a^2c$
X-ray density (g cm^{-3})	5.296	5.106	Cell mass / V
Moment at 0 K (μ_B per f.u.)	20	20	Gorter model [3]
σ_0 at 0 K (emu g^{-1})	100.5	105.2	$n\mu_B N_A/M$
M_s at 300 K (emu cm^{-3})	381	378	$\sigma_s\rho$, σ_s = 72, 74 emu g^{-1}
K_1 at 300 K (10^6 erg cm^{-3})	3.3	3.5	[28]
$H_A = 2K_1/M_s$ (kOe)	17.3	18.5	Computed
H_c limit, $0.48H_A$ (kOe)	8.3	8.9	[48]
D_c, single-domain (µm)	0.55	0.58	[53, 55]
D_{sp}, 300 K (nm)	8.4	8.3	$K_1V = 25k_BT$

Exchange stiffness $A \approx 6$ pJ m^{-1} assumed for both compounds [53].

Annual Methodological Archive Research Review
http://amresearchreview.com/index.php/Journal/about
Volume 4, Issue 2(2026)

Online ISSN 3007-3197
Print ISSN 3007-3189
http://amresearchreview.com/index.php/Journal/about

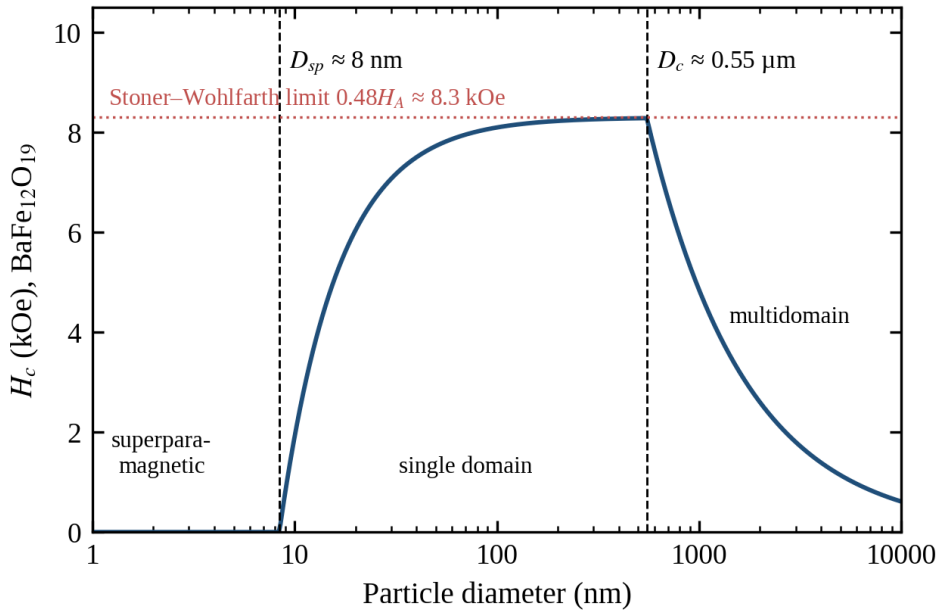


Figure 6. Schematic dependence of coercivity on particle diameter for $BaFe_{12}O_{19}$, drawn with the thresholds computed in this work ($D_{sp} \approx 8$ nm, $D_c \approx 0.55$ µm) and the Stoner–Wohlfarth limit [48]. In the single-domain range the curve follows the thermal-activation form $H_c = 0.48H_A[1 - (D_{sp}/D)^{3/2}]$; the multidomain branch is illustrative.

Effect of synthesis route

Figure 4b places the reported routes on a common temperature scale. Hydrothermal synthesis forms BaM at 150–240 °C [20], co-precipitation at 925 °C [18] and sol–gel auto-combustion between 900 and 1200 °C [23], while highly substituted compositions still need about 1200 °C to incorporate Al fully [16]. The order follows the length scale of mixing: the closer the cations are mixed in the precursor, the shorter the diffusion distance and the lower the temperature at which the M phase forms. Low temperature, however, is not the same as good magnetic performance. The hydrothermal particles fall below D_{sp} and are superparamagnetic [37], and sol–gel Al-SrM calcined at 900 °C still contains α-Fe_2O_3, which disappears only after calcination at higher temperature [23]. The anion chemistry of the precursor also matters: in sol–gel fibres, retained halide delayed the formation of BaM and SrM, and a halide-free nitrate sol lowered the formation temperature by 200 °C and reduced the grain size [39]. The practical window for hard M-type ferrites is therefore the calcination range that removes secondary phases while keeping grains below D_c.

Substitution and the magnetisation–coercivity trade-off

The Al-substituted SrM data (Figure 7a) show the trade-off most clearly. As x increases from 1.5 to 4, M_s falls from 47.5 to 12.9 emu g^{-1}, a 73% loss, while H_c doubles from 9.1 to 18.5 kOe [16]. The rise of H_c accelerates above x = 3, where M_s drops below about 22 emu g^{-1} and $H_A = 2K_1/M_s$ grows quickly. Only single-domain particles show this gain: when grain growth during the high-temperature anneal pushes particles above D_c, the coercivity drops abruptly [16]. The Ca–Al series (Figure 7b) shows the cost in

Annual Methodological Archive Research Review
http://amresearchreview.com/index.php/Journal/about
Volume 4, Issue 2(2026)

Online ISSN 3007-3197
Print ISSN 3007-3189
http://amresearchreview.com/index.php/Journal/about

thermal stability. Between x = 1.5 and 4.5, T_C falls from 648 to 466 K, about 61 K per unit of x, while the cell volume contracts from 679.3 to 654.2 $Å^3$ [21]. In the same work, H_c for x = 5.5 reached 42 kOe at 180 K, and both H_c and the resonance frequency peaked at lower temperatures as Al content increased [21]. A designer who chooses these materials for millimetre-wave absorbers must therefore check that the operating temperature lies well below a reduced T_C.

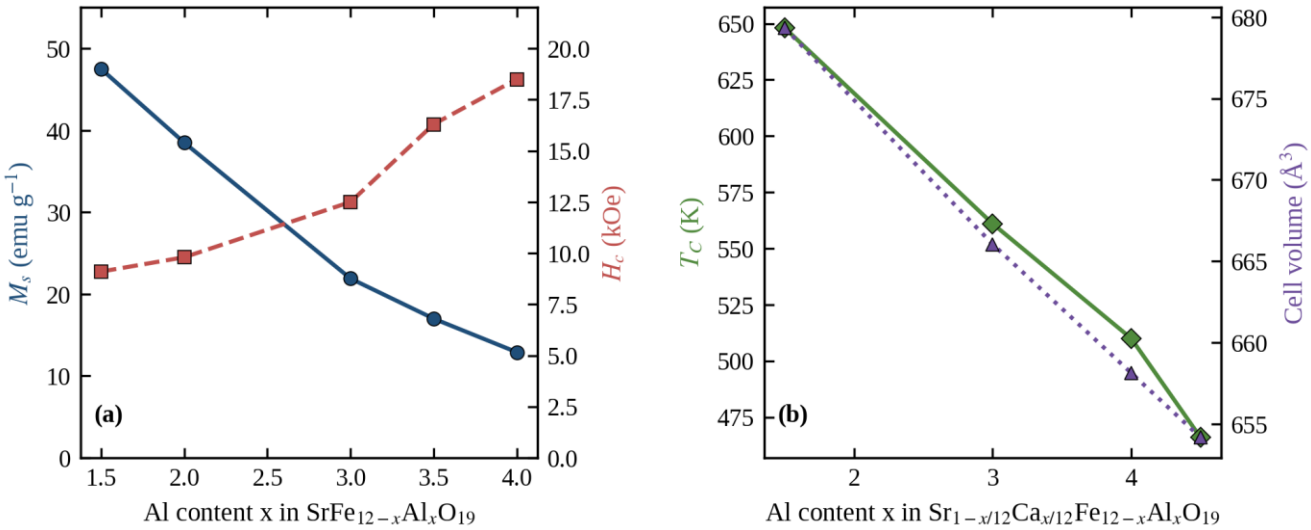


Figure 7. (a) Saturation magnetisation and coercivity of $SrFe_{12-x}Al_xO_{19}$ as a function of Al content, plotted from the data of Trusov et al. [16]. (b) Curie temperature and unit-cell volume of $Sr_{1-x/12}Ca_{x/12}Fe_{12-x}Al_xO_{19}$, plotted from Gorbachev et al. [21]; cell volumes were recalculated from the reported lattice parameters.

La–Co substitution follows a different path. It raises the anisotropy without the large loss of magnetisation that Al causes, because Co^{2+} on $4f_2$ adds single-ion anisotropy and the La^{3+}/Co^{2+} pair keeps the charge balanced [19, 40]. This makes it the preferred choice for permanent magnets, where the energy product depends on both M_s and H_c, whereas Al substitution is better suited to applications that need anisotropy field more than magnetisation, such as high-frequency absorbers [17, 24].

Property map and application regimes

Figure 8 places the compiled data on a single M_s–H_c map. Three groups separate clearly. Co_2X and Co_2U sol–gel fibres have high magnetisation (45–52 emu g^{-1}) and coercivities below 1 kOe [27], the soft behaviour required for inductors and gigahertz permeability. Unsubstituted BaM and SrM sol–gel fibres sit at 58–65 emu g^{-1} and 5.0–5.5 kOe [39], the regime of permanent magnets, recording and self-biased microwave devices. Al and Ca–Al substituted SrM extend along a line towards 13–14 emu g^{-1} and 18–21 kOe [16], where they meet ε-Fe_2O_3 (15 emu g^{-1}, 20 kOe) and Rh-substituted ε-Fe_2O_3 (7 emu g^{-1}, 27 kOe) [16, 56]. The hexaferrites reach this regime with higher magnetisation than the ε-oxides and from a simpler citrate process [16]. The map also shows the empty region at high magnetisation and high coercivity; no single-phase ferrite reaches it, which is the motivation for exchange-coupled hard–soft composites [4, 6].

Annual Methodological Archive Research Review
http://amresearchreview.com/index.php/Journal/about
Volume 4, Issue 2(2026)

Online ISSN 3007-3197
Print ISSN 3007-3189
http://amresearchreview.com/index.php/Journal/about

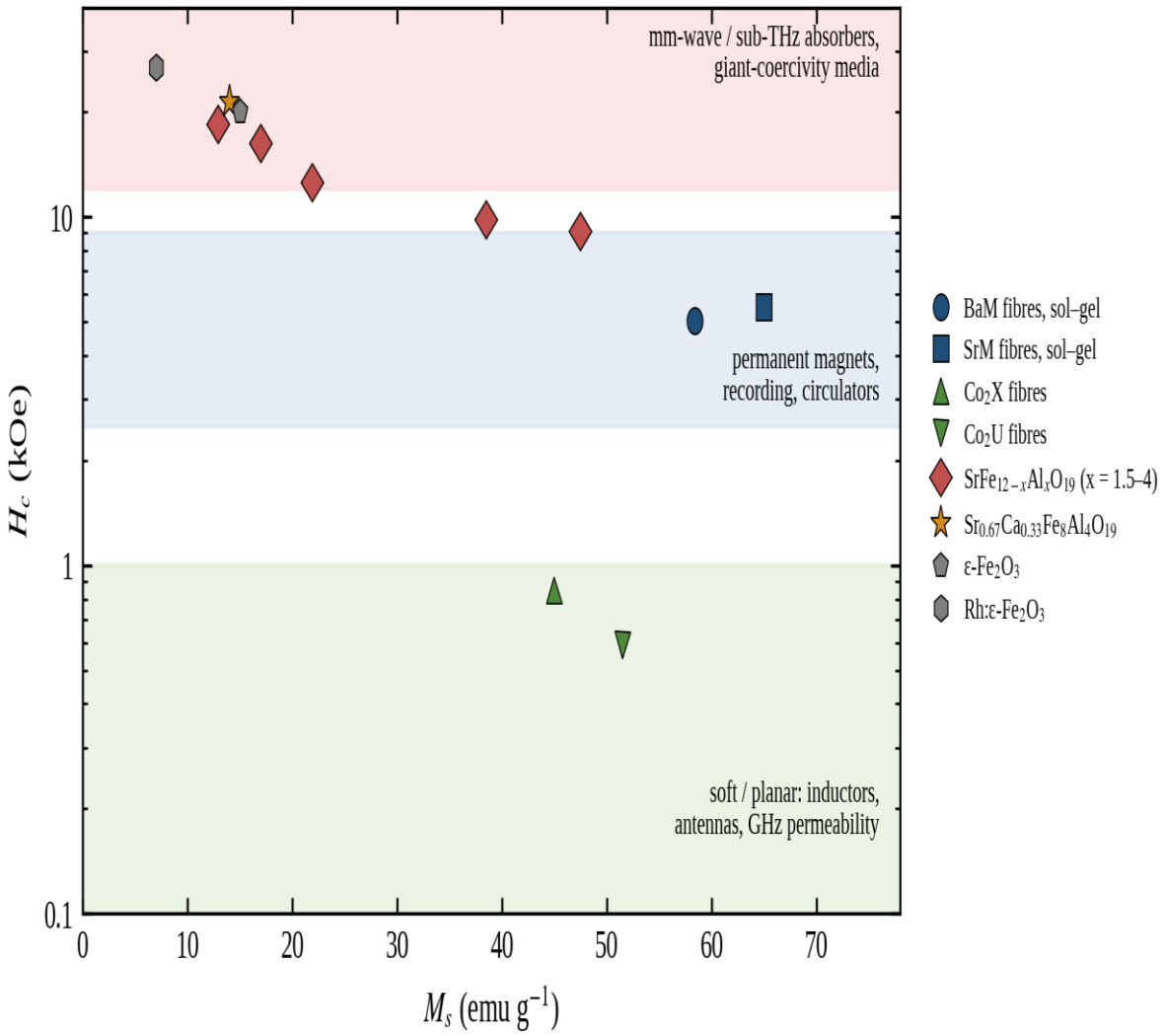


Figure 8. Saturation magnetisation versus room-temperature coercivity for representative hexaferrites and ε-Fe_2O_3, compiled from the literature: BaM and SrM fibres [39], Co_2X and Co_2U fibres [27], $SrFe_{12-x}Al_xO_{19}$ and $Sr_{0.67}Ca_{0.33}Fe_8Al_4O_{19}$ [16], and ε-Fe_2O_3 and Rh:ε-Fe_2O_3 as quoted in [16, 56]. Shaded bands indicate application regimes.

Lattice contraction and diffraction shifts on substitution

Because Al^{3+} (ionic radius about 0.535 Å in octahedral coordination) is smaller than high-spin Fe^{3+} (0.645 Å), substitution contracts the lattice. In the Ca–Al series, *a* falls by 1.87% and *c* by 1.64% between x = 0 and x = 4.5 (Figure 9b), using the reference SrM values and the reported data [21, 26]. The computed consequence for diffraction is a systematic shift to higher angles that grows with the diffraction angle (Figure 9a). At x = 4.5 the (114) reflection moves by 0.65°, the (2 0 11) reflection by 1.10° and the (220) reflection by 1.35°. These shifts are large enough to be followed with laboratory diffractometers and give a simple check of whether the nominal Al content has entered the lattice. A sample whose peaks do not shift as expected probably contains unreacted

Annual Methodological Archive Research Review
http://amresearchreview.com/index.php/Journal/about
Volume 4, Issue 2(2026)

Online ISSN 3007-3197
Print ISSN 3007-3189
http://amresearchreview.com/index.php/Journal/about

Al in an amorphous or secondary phase, which is the situation reported for hydrothermal and solid-salt-matrix syntheses [36].

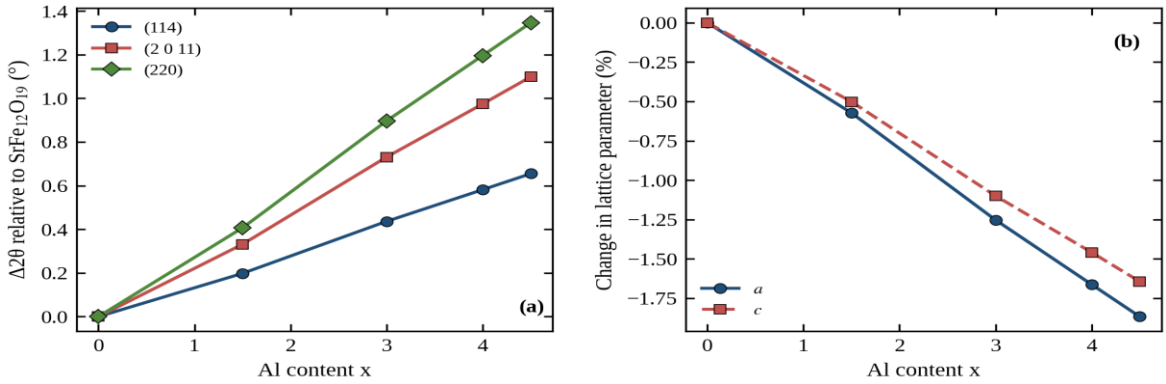


Figure 9. (a) Computed shift of the (114), (2 0 11) and (220) reflections (Cu Kα) of $Sr_{1-x/12}Ca_{x/12}Fe_{12-x}Al_xO_{19}$ relative to $SrFe_{12}O_{19}$, obtained from reported lattice parameters [21, 26]. (b) Relative change of the lattice parameters a and c with Al content.

Sublattice dilution and site preference

Figure 10 compares the measured relative magnetisation of $SrFe_{12-x}Al_xO_{19}$ [16] with two limiting cases of the Gorter model. If every Al ion replaced Fe on a spin-up site, the net moment would fall as $(20 - 5x)\ \mu_B$ and reach zero at x = 4. If every Al ion went to a spin-down site, the moment would instead rise. The measured values follow the first line closely up to x = 2 (0.64 and 0.52 compared with 0.63 and 0.50) but lie well above it at x = 3.5 and 4 (0.23 and 0.17 compared with 0.13 and 0). The simplest explanation is that Al first enters spin-up sites and then increasingly enters spin-down sites at high x, which agrees with the neutron result that Al occupies 2a and 12k at low content and also 4e and 4f at higher content [36]. The comparison is approximate, because the model refers to 0 K and the data to room temperature, and the Curie temperature falls as x increases [21], but the direction and size of the deviation are consistent with the structural evidence.

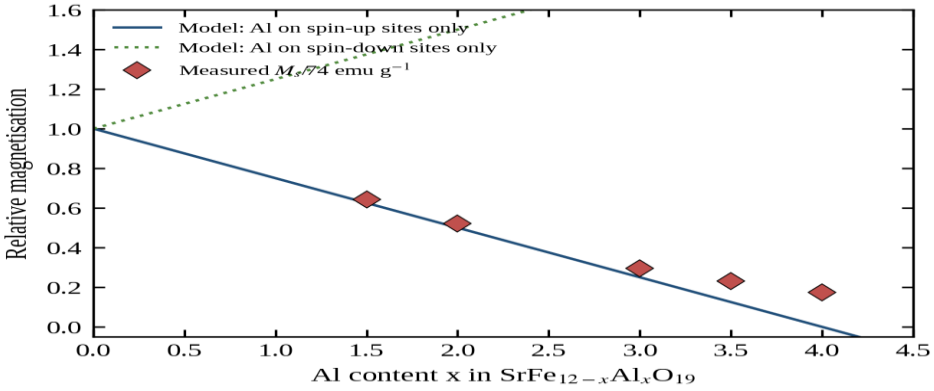


Figure 10. Relative magnetisation of $SrFe_{12-x}Al_xO_{19}$: measured room-temperature values [16] normalised to 74 emu g^{-1} [3], compared with the collinear Gorter model for Al placed only on spin-up or only on spin-down Fe sites (computed in this work).

Annual Methodological Archive Research Review
http://amresearchreview.com/index.php/Journal/about
Volume 4, Issue 2(2026)

Online ISSN 3007-3197
Print ISSN 3007-3189
http://amresearchreview.com/index.php/Journal/about

Resonance frequencies and microwave bands

The computed anisotropy fields place the natural resonance of unsubstituted BaM and SrM at 48.4 and 51.8 GHz (Figure 11, Table 6), in the V band. This is the property that makes M-type ferrites suitable for self-biased circulators and absorbers in the 30–60 GHz range without a large external magnet [8, 9]. Reported resonance frequencies of heavily substituted SrM are about three to six times higher. $SrFe_8Al_4O_{19}$ particles resonate at 149–164 GHz [57], Ca–Al co-substituted samples at 160–250 GHz at room temperature [17], and the x = 5.5 composition at 297 GHz at 180 K [21]. Inverting the resonance condition gives effective anisotropy fields of 53–106 kOe, three to six times that of SrM. ε-Fe_2O_3 and its Rh-substituted form, which have long been the reference materials for millimetre-wave absorption, resonate at 182–209 GHz [56]. The substituted hexaferrites therefore cover the same band and extend beyond it, with higher magnetisation and a simpler synthesis [16, 24].

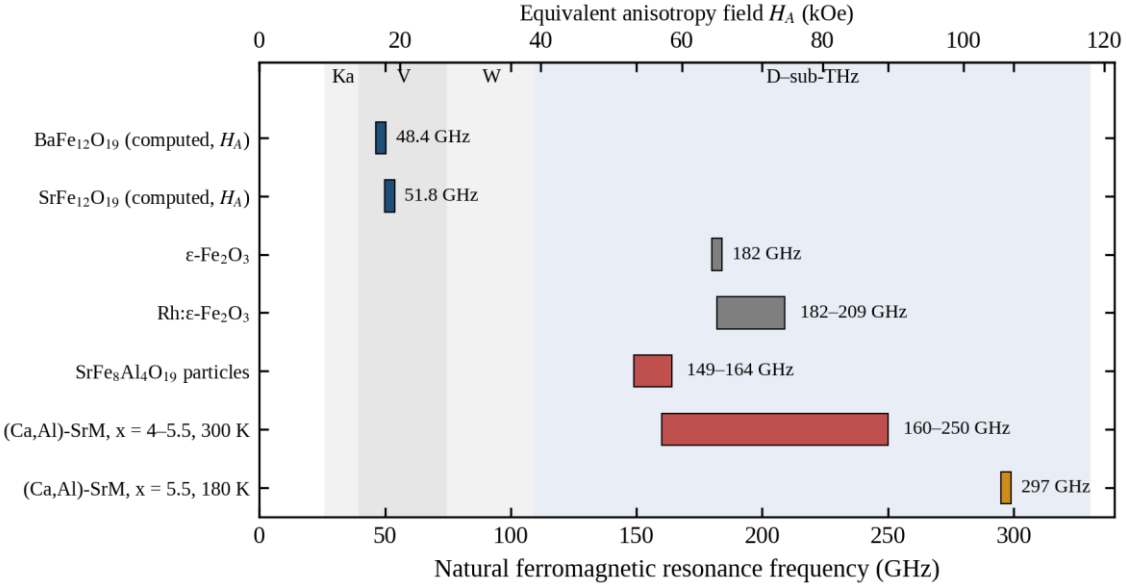


Figure 11. Natural ferromagnetic resonance frequencies: values for $BaFe_{12}O_{19}$ and $SrFe_{12}O_{19}$ computed in this work from $f_r = (\gamma/2\pi)H_A$, and reported values for $SrFe_8Al_4O_{19}$ [57], (Ca,Al)-substituted SrM [17, 21] and ε-Fe_2O_3 and Rh:ε-Fe_2O_3 [56]. The upper axis gives the equivalent anisotropy field; shaded regions mark waveguide bands.

Table 6. Microwave and permanent-magnet figures of merit computed for unsubstituted M-type ferrites.

Quantity	BaM	SrM	Relation
Anisotropy field H_A (kOe)	17.3	18.5	$2K_1/M_s$
Natural resonance f_r (GHz)	48.4	51.8	$(\gamma/2\pi)H_A$, $\gamma/2\pi$ = 2.80 GHz kOe^{-1}
Saturation polarisation J_s (kG)	4.79	4.75	$4\pi M_s$
$(BH)_{max}$ upper bound (MGOe)	5.73	5.64	$J_s^2/4$ [53]

Annual Methodological Archive Research Review
http://amresearchreview.com/index.php/Journal/about
Volume 4, Issue 2(2026)

Online ISSN 3007-3197
Print ISSN 3007-3189
http://amresearchreview.com/index.php/Journal/about

Quantity	BaM	SrM	Relation
$(BH)_{max}$ upper bound (kJ m^{-3})	45.6	44.9	1 MGOe = 7.958 kJ m^{-3}
H_c limit / H_A	0.48	0.48	Random assembly [48]

Values computed in this work from the room-temperature constants in Table 5.

Energy-product limits for permanent magnets

For permanent magnets the relevant figure of merit is the maximum energy product. For an ideal, fully dense and fully aligned magnet with a square loop, $(BH)_{max}$ cannot exceed $J_s^2/4$ [53]. With the room-temperature magnetisation of Table 5 this gives 5.73 MGOe (45.6 kJ m^{-3}) for BaM and 5.64 MGOe (44.9 kJ m^{-3}) for SrM (Table 6). The bound is set by magnetisation, not coercivity, because both compounds already have H_c well above $J_s/2 \approx 2.4$ kG once particles are single-domain. Two consequences follow. First, substitutions that raise H_c at the expense of M_s, such as Al, lower the attainable energy product and are of little use for magnets [16]. Second, improvements must come from raising M_s and remanence: La–Co substitution, which raises anisotropy with little loss of magnetisation, and better alignment and density in sintered bodies are the routes that have improved commercial grades [6, 19]. Exchange-coupled composites with a soft phase are the only route that can, in principle, exceed the single-phase bound [5, 6].

Discussion

Why synthesised hexaferrites operate below their intrinsic limits

Answering RQ1, the evidence shows that unsubstituted M-type ferrites typically reach 60–65% of their Stoner–Wohlfarth coercivity and about 80–90% of their room-temperature magnetisation. The loss of coercivity is extrinsic. Particles outside the window between D_{sp} and D_c, surface damage from milling, and magnetostatic interaction in dense compacts all lower H_c [18, 22]. The loss of magnetisation comes mainly from secondary phases and from reduced order at particle surfaces, which becomes significant when particles are only a few cells thick [37]. The single-domain window for M-type ferrites is wide, covering almost two orders of magnitude in diameter, so it can be reached with several routes. The difficulty lies in keeping the size distribution narrow while removing secondary phases, because both depend on the same calcination step.

The comparison between computed and measured values is also a test of the reference parameters themselves. The computed X-ray densities agree with the accepted values for BaM and SrM, and the computed resonance frequencies of about 48 and 52 GHz fall in the range in which M-type ferrites are used as self-biased microwave materials [8, 9]. The single-domain diameter of about 0.55 µm agrees with the critical size of about 500 nm reported for SrM [16]. These checks support using the same framework to judge new results: a coercivity close to $0.48H_A$ indicates a well-dispersed, single-domain and defect-free powder, while a value far below it points to one of the extrinsic causes discussed above.

Annual Methodological Archive Research Review
http://amresearchreview.com/index.php/Journal/about
Volume 4, Issue 2(2026)

Online ISSN 3007-3197
Print ISSN 3007-3189

http://amresearchreview.com/index.php/Journal/about

Strategies along the trade-off

For RQ2, the compiled data separate strategies by their purpose. Where M_s and H_c both matter, as in permanent magnets, La–Co substitution and careful sintering give the best balance [6, 19]. Where anisotropy field matters most, as in absorbers and self-biased devices above about 50 GHz, heavy Al or Ca–Al substitution is the most effective lever, provided the synthesis gives single-domain particles and atomic-scale mixing [16, 17, 36]. The finding that Al enters the lattice effectively only in the sol–gel route, but not in hydrothermal or solid-salt-matrix syntheses [36], shows that route and substitution cannot be optimised separately. For soft, planar ferrites the main target is phase purity of Y, Z or U, which is harder than for M because the formation windows are narrow and the phases intergrow [4, 27].

Characterisation pitfalls

Several practices limit comparison across studies. Crystallite sizes from the Scherrer equation measure coherent diffraction domains and are not particle sizes, and for platelet-shaped hexaferrites the broadening also depends on direction [43, 44]. M_s values for strongly anisotropic samples are underestimated unless they are measured at fields well above H_A or extrapolated with the law of approach to saturation; Trusov *et al.* report magnetisation at 50 and 70 kOe for exactly this reason [16]. A few per cent of α-Fe_2O_3 can lower M_s measurably while remaining near the detection limit of laboratory diffraction, so phase fractions should be refined rather than judged by eye [23, 42]. Infrared bands near 400–600 cm^{-1} confirm metal–oxygen bonding [45] but cannot by themselves separate the hexaferrite from spinel or hematite impurities. Raman spectroscopy, whose modes in BaM have been assigned in detail [46], and Mössbauer spectroscopy are more specific.

Implications for applications

For permanent magnets the main opportunity is to approach the coercivity limit in dense, aligned bodies without losing remanence, which requires grains close to but below D_c and low-temperature densification [6]. For microwave devices the anisotropy field sets the operating band, so the substituted SrM phases with natural resonance in the sub-terahertz range open frequencies that conventional ferrites cannot reach [17, 21]. Their lower T_C narrows the thermal margin, and future device studies should report how the resonance shifts with temperature. For magnetoelectric devices the open problem is stability: room-temperature effects exist in Z-type and Sc-doped M-type compounds [13, 14, 50], but practical devices need polycrystalline, low-leakage materials that work at low magnetic fields [15].

Placing hexaferrites against competing hard magnetic materials clarifies where they are, and are not, the right choice (Figure 12, Table 7). $Nd_2Fe_{14}B$ has more than three times the saturation polarisation of BaM, which raises the upper bound of its energy product by about an order of magnitude, but its Curie temperature of 585 K is lower than that of the M-type ferrites and its anisotropy falls quickly on heating [5, 53]. $SmCo_5$ combines high anisotropy with a high Curie temperature but depends on samarium and cobalt [53]. The hexaferrites are the only materials in the comparison

Annual Methodological Archive Research Review
http://amresearchreview.com/index.php/Journal/about
Volume 4, Issue 2(2026)

Online ISSN 3007-3197
Print ISSN 3007-3189
http://amresearchreview.com/index.php/Journal/about

that are oxides, which gives them high electrical resistivity, low eddy-current loss and chemical stability without coatings [4, 5]. ε-Fe_2O_3 reaches coercivities near 20 kOe but has a magnetisation of only about 15 emu g^{-1} and is difficult to make as a single phase in large quantities [16, 56]. The substituted hexaferrites now cover a similar coercivity range from a scalable route, which strengthens the case for ferrites in high-frequency and high-coercivity niches rather than in high-energy-product magnets.

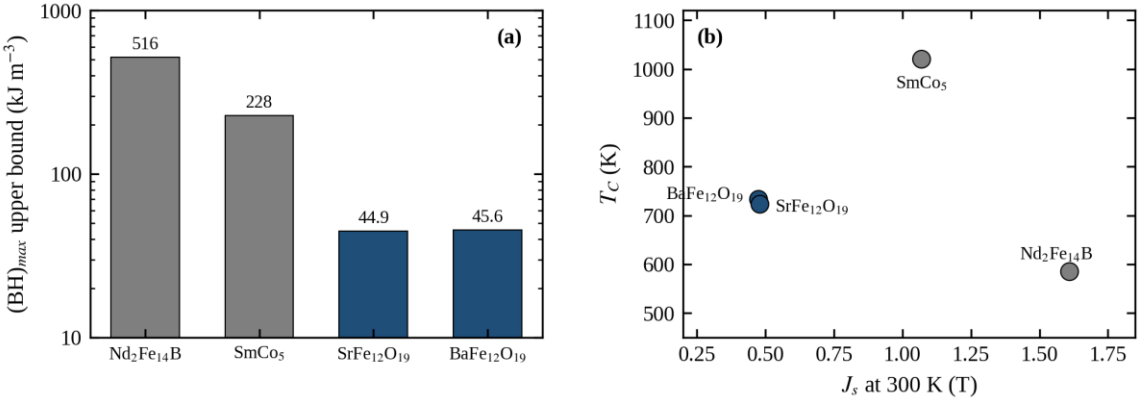


Figure 12. (a) Upper bound of the maximum energy product, $J_s^2/4\mu_0$, and (b) saturation polarisation versus Curie temperature for hexaferrites and rare-earth magnets. Hexaferrite values computed in this work from [28]; $Nd_2Fe_{14}B$ and $SmCo_5$ from [5, 53].

Table 7. Intrinsic room-temperature properties of hexaferrites compared with other hard magnetic materials.

Material	J_s (T)	$\mu_0 H_A$ (T)	T_C (K)	$(BH)_{max}$ bound (kJ m^{-3})	Source
$BaFe_{12}O_{19}$	0.48	1.73	723	45.6	This work, from [28]
$SrFe_{12}O_{19}$	0.48	1.85	733	44.9	This work, from [28]
$Nd_2Fe_{14}B$	1.61	7.6	585	516	[5, 53]
$SmCo_5$	1.07	40	1020	228	[5, 53]
ε-Fe_2O_3	(15 emu g^{-1})	$H_c \approx 2.0$	–	–	[16, 56]

Upper bounds of $(BH)_{max}$ computed as $J_s^2/4\mu_0$. For ε-Fe_2O_3 the mass magnetisation and coercivity are given because volume data are not compared on the same basis.

Cost, sustainability and supply

Hexaferrites are made from iron oxide and barium or strontium carbonate, which are abundant and inexpensive, and they need no rare earths in their basic form [5, 58]. This matters because the supply of heavy rare earths for Nd–Fe–B magnets is concentrated and volatile, and many applications, such as small motors, sensors and loudspeakers, do not need the energy product of rare-earth magnets [6, 58]. The gap between ferrites (below about 5.7 MGOe) and Nd–Fe–B is the target of research on improved ferrites and on composites [58]. La–Co substitution reintroduces a light rare earth and cobalt,

Annual Methodological Archive Research Review
http://amresearchreview.com/index.php/Journal/about
Volume 4, Issue 2(2026)

Online ISSN 3007-3197
Print ISSN 3007-3189
http://amresearchreview.com/index.php/Journal/about

so the compositions that avoid both, such as optimised Ca–Al or Ca–Al–Cr substituted SrM, are of interest where cost and supply security matter more than energy product [6, 16]. Chemical routes add the cost of nitrates and organic fuels and release NO_x and CO_2 during combustion, which should be weighed against their lower calcination temperature [4]. Table 8 brings these considerations together by matching application requirements to the hexaferrites best suited to them.

Table 8. Application requirements and the hexaferrites best matched to them.

Application	Key requirement	Preferred materials	Main constraint
Bonded and sintered permanent magnets	High M_r, H_c near single-domain limit, low cost	BaM, SrM, La–Co SrM [6, 19]	$(BH)_{max} \leq 5.7$ MGOe
Self-biased circulators, isolators	High H_A, c-axis texture, low FMR linewidth	Oriented BaM films and compacts [51, 52]	Film thickness and texture
Millimetre-wave and sub-THz absorbers	f_r in target band, adequate M_s	Al and Ca–Al substituted SrM [17, 21]	Low M_s, reduced T_C
GHz inductors and antenna substrates	High permeability in plane, low loss	Co_2Z, Co_2Y [4, 9]	Phase purity, sintering temperature
Magnetic recording	Fine, uniform platelets; controlled H_c	BaM particles [10, 11]	Particle-size distribution
Magnetoelectric memory and sensors	Room-temperature conical order, low switching field	Co_2Z, Sc-doped BaM [13, 14, 50]	Weak coupling; single crystals

Recommendations for reporting

In answer to RQ3, Table 9 lists the information that would allow results to be compared directly. None of the items requires new equipment; they require the reporting of quantities that most laboratories already measure.

Table 9. Recommended minimum reporting for hexaferrite synthesis and characterisation studies.

Item	Recommended practice	Reason
Precursor chemistry	State salts, chelating agent, metal-to-fuel ratio and anions	Anion chemistry shifts formation temperature [39]
Thermal history	Give ramp rate, dwell time and atmosphere for every step	Phase purity and grain size depend on both [16, 23]
Phase analysis	Rietveld refinement with weight fractions of all phases	Small α-Fe_2O_3 fractions lower M_s [42]
Size	Report microscopy particle size with distribution as well as crystallite size	Line broadening measures coherent domains [43]
Magnetisation	Give maximum field and use law of approach for M_s	Anisotropic samples saturate slowly [16]
Units	Use SI or cgs consistently and state conversions	Avoids errors when values are compiled

Annual Methodological Archive Research Review
http://amresearchreview.com/index.php/Journal/about
Volume 4, Issue 2(2026)

Online ISSN 3007-3197
Print ISSN 3007-3189
http://amresearchreview.com/index.php/Journal/about

Item	Recommended practice	Reason
Reference limits	Compare H_c with $0.48H_A$ using stated K_1 and M_s	Shows how far extrinsic factors limit performance [48]
Site occupancy	Use Mössbauer or neutron data when claiming site preference	Diffraction with X-rays alone cannot separate Fe and Al well [29, 36]

Limitations

This study has limitations. The numerical comparisons rely on published values, which come from different instruments, fields and sample forms (powders, fibres, single crystals), and these differences cannot be fully removed by unit conversion. The structural simulation uses ideal site positions and full occupancy, so it does not include the split 2b site, preferred orientation or the anisotropic broadening of real platelets [26]. The magnetic estimates use one-constant anisotropy and an assumed exchange stiffness, which is adequate for limits and thresholds but not for detailed loop shapes, and the resonance estimates neglect demagnetising and shape effects, which can shift f_r by several gigahertz in platelets. The dilution model assumes collinear spins and ignores canting at high substitution. Finally, the selection of studies favours well-characterised work and may under-represent the much larger number of reports with incomplete characterisation.

Future work

Four directions follow from the evidence. First, controlled-size synthesis of substituted SrM in the window between D_{sp} and D_c, combined with field alignment, could approach the coercivity limits in bulk parts [17]. Second, joint neutron and Mössbauer studies of site occupancy across routes would establish which substitutions are effective in practice rather than only in nominal composition [36]. Third, exchange-coupled composites of hard M-type and soft spinel or Y/Z phases remain the most direct way to reach the empty high-M_s, high-H_c region of Figure 8 [4]. Fourth, room-temperature magnetoelectric hexaferrites need studies on polycrystalline films and on reliability under repeated switching before they can be used in memory or sensor devices [15, 50].

Practical guidance for experimental studies

For researchers planning an experimental study, the evidence suggests a sequence. Start from the target application in Table 8 and define the required anisotropy field, magnetisation and operating temperature. Choose the substitution scheme that moves the material in the required direction along the trade-off in Figure 8, then choose a route that gives atomic-scale mixing for that scheme, which for heavy substitution means a sol–gel or citrate route [16, 36]. Use the computed fingerprint in Table 4 and the expected peak shifts in Figure 9 to verify incorporation, quantify secondary phases by Rietveld refinement, and measure particle size by microscopy. Finally, compare the measured H_c with $0.48H_A$ and M_s with the dilution model, so that the gap to the intrinsic limit is known and can be reduced in the next iteration [42, 48].

Annual Methodological Archive Research Review
http://amresearchreview.com/index.php/Journal/about
Volume 4, Issue 2(2026)

Online ISSN 3007-3197
Print ISSN 3007-3189

http://amresearchreview.com/index.php/Journal/about

Conclusion

Hexaferrites remain among the most useful magnetic materials because their crystal structure provides strong anisotropy and high resistivity in an inexpensive, stable oxide. This study shows that their usable properties are set mainly by synthesis. Using published structural and magnetic constants, we computed reference diffraction patterns, densities and sublattice moments for $BaFe_{12}O_{19}$ and $SrFe_{12}O_{19}$, and derived anisotropy fields of 17.3 and 18.5 kOe, coercivity limits of 8.3 and 8.9 kOe and a single-domain window from about 8 nm to 0.55 µm. Reported unsubstituted M-type ferrites reach about 60–65% of this coercivity limit, and the gap is explained by particle size, secondary phases and surface damage. Chemical routes lower the formation temperature from above 900 °C to as little as 150 °C but give useful hard magnets only when particles stay within the single-domain window. Aluminium and calcium–aluminium substitution move SrM along a clear trade-off, from 47.5 emu g^{-1} and 9.1 kOe to 12.9 emu g^{-1} and 18.5 kOe, and up to 36 kOe at higher substitution, at the cost of a Curie temperature that falls by about 60 K per unit of x. Peak shifts computed from reported lattice parameters, together with the deviation of measured magnetisation from a sublattice-dilution model, indicate that Al first occupies spin-up sites and then spin-down sites at high content. The resulting anisotropy fields move the natural resonance from about 50 GHz in unsubstituted ferrites to 150–300 GHz, whereas the energy product of single-phase ferrite magnets remains bounded at about 5.7 MGOe by magnetisation. Plotted together, the compiled data define three application regimes and an unoccupied region at high magnetisation and coercivity. Consistent reporting of phase fractions, particle-size distributions, measuring fields and units, as set out in Table 9, would make future results comparable and would speed up the design of hexaferrites for magnets, microwave devices and magnetoelectric applications.

Abbreviations

Table 10. Abbreviations and symbols used in this paper.

Symbol	Meaning	Symbol	Meaning
BaM, SrM	$BaFe_{12}O_{19}$, $SrFe_{12}O_{19}$ (M-type)	M_s, σ_s	Saturation magnetisation (volume, mass)
W, X, Y, Z, U	Hexaferrite structure types	M_r	Remanent magnetisation
R, S, T	Structural blocks of the hexaferrites	H_c	Coercivity
12k, 2a, 2b, $4f_1$, $4f_2$	Fe sites in the M structure	H_A, K_1	Anisotropy field, first anisotropy constant
XRD	X-ray diffraction	T_C	Curie temperature
FTIR	Fourier-transform infrared spectroscopy	D_c, D_{sp}	Single-domain and superparamagnetic diameters
VSM, SQUID	Vibrating-sample and SQUID magnetometry	f_r	Natural ferromagnetic resonance frequency

Online ISSN 3007-3197
Print ISSN 3007-3189
http://amresearchreview.com/index.php/Journal/about

Symbol	Meaning	Symbol	Meaning
FMR, VNA	Ferromagnetic resonance, vector network analyser	J_s	Saturation polarisation, $4\pi M_s$
NPD	Neutron powder diffraction	$(BH)_{max}$	Maximum energy product
ME	Magnetoelectric	μ_B	Bohr magneton

Declarations

Funding. This research received no specific grant from any funding agency in the public, commercial or not-for-profit sectors.

Conflict of interest. The authors declare no conflict of interest.

Data availability. All literature data used in the figures are taken from the cited sources. The computed diffraction patterns, magnetic parameters and plotting scripts are available from the corresponding author on reasonable request.

Author contributions. Conceptualisation, literature analysis, computation, visualisation and writing were carried out by the authors, who read and approved the final manuscript.

References

[1] Went JJ, Rathenau GW, Gorter EW, van Oosterhout GW. Ferroxdure, a class of new permanent magnet materials. Philips Tech Rev. 1952;13:194–208.
[2] Braun PB. The crystal structures of a new group of ferromagnetic compounds. Philips Res Rep. 1957;12:491–548.
[3] Smit J, Wijn HPJ. Ferrites. Eindhoven: Philips Technical Library; 1959.
[4] Pullar RC. Hexagonal ferrites: a review of the synthesis, properties and applications of hexaferrite ceramics. Prog Mater Sci. 2012;57(7):1191–1334.
[5] Coey JMD. Hard magnetic materials: a perspective. IEEE Trans Magn. 2011;47(12):4671–4681.
[6] de Julián Fernández C, Sangregorio C, de la Figuera J, Belec B, Makovec D, Quesada A. Progress and prospects of hard hexaferrites for permanent magnet applications. J Phys D Appl Phys. 2021;54(15):153001.
[7] Özgür Ü, Alivov Y, Morkoç H. Microwave ferrites, part 1: fundamental properties. J Mater Sci Mater Electron. 2009;20(9):789–834.
[8] Harris VG, Geiler A, Chen Y, Yoon SD, Wu M, Yang A, et al. Recent advances in processing and applications of microwave ferrites. J Magn Magn Mater. 2009;321(14):2035–2047.
[9] Harris VG. Modern microwave ferrites. IEEE Trans Magn. 2012;48(3):1075–1104.
[10] Kubo O, Ido T, Yokoyama H. Properties of Ba ferrite particles for perpendicular magnetic recording media. IEEE Trans Magn. 1982;18(6):1122–1124.
[11] Lantz MA, Furrer S, Cherubini G, et al. 123 Gbit/in² recording areal density on barium ferrite tape. IEEE Trans Magn. 2015;51(11):3101304.
[12] Kimura T, Lawes G, Ramirez AP. Electric polarization rotation in a hexaferrite with long-wavelength magnetic structures. Phys Rev Lett. 2005;94(13):137201.
[13] Kitagawa Y, Hiraoka Y, Honda T, Ishikura T, Nakamura H, Kimura T. Low-field magnetoelectric effect at room temperature. Nat Mater. 2010;9(10):797–

Online ISSN 3007-3197
Print ISSN 3007-3189
http://amresearchreview.com/index.php/Journal/about

802.

[14] Tokunaga Y, Kaneko Y, Okuyama D, Ishiwata S, Arima T, Wakimoto S, et al. Multiferroic M-type hexaferrites with a room-temperature conical state and magnetically controllable spin helicity. Phys Rev Lett. 2010;105(25):257201.

[15] Kimura T. Magnetoelectric hexaferrites. Annu Rev Condens Matter Phys. 2012;3:93–110.

[16] Trusov LA, Gorbachev EA, Lebedev VA, Sleptsova AE, Roslyakov IV, Kozlyakova ES, et al. Ca–Al double-substituted strontium hexaferrites with giant coercivity. Chem Commun. 2018;54(5):479–482.

[17] Gorbachev EA, Trusov LA, et al. Hexaferrite materials displaying ultra-high coercivity and sub-terahertz ferromagnetic resonance frequencies. Mater Today. 2020;32:13–18.

[18] Haneda K, Miyakawa C, Kojima H. Preparation of high-coercivity BaFe12O19. J Am Ceram Soc. 1974;57(8):354–357.

[19] Kools F, Morel A, Grössinger R, Le Breton JM, Tenaud P. LaCo-substituted ferrite magnets, a new class of high-grade ceramic magnets; intrinsic and microstructural aspects. J Magn Magn Mater. 2002;242–245:1270–1276.

[20] Primc D, Makovec D, Lisjak D, Drofenik M. Hydrothermal synthesis of ultrafine barium hexaferrite nanoparticles and the preparation of their stable suspensions. Nanotechnology. 2009;20(31):315605.

[21] Gorbachev EA, Kozlyakova ES, Alyabyeva LN, Ahmed A, Trusov LA. Hard ferrite magnetic insulators revealing giant coercivity and sub-terahertz natural ferromagnetic resonance at 5–300 K. Mater Horiz. 2023;10(5):1842–1847.

[22] Kojima H. Fundamental properties of hexagonal ferrites with magnetoplumbite structure. In: Wohlfarth EP, editor. Ferromagnetic Materials. Vol. 3. Amsterdam: North-Holland; 1982. p. 305–391.

[23] Torkian S, Ghasemi A, Shoja Razavi R, Tavoosi M. Structural and magnetic properties of high coercive Al-substituted strontium hexaferrite nanoparticles. J Supercond Nov Magn. 2016;29(6):1627–1640.

[24] Gorbachev EA, Trusov LA, et al. Design of modern magnetic materials with giant coercivity. Russ Chem Rev. 2021;90(10):1287–1329.

[25] Townes WD, Fang JH, Perrotta AJ. The crystal structure and refinement of ferrimagnetic barium ferrite, BaFe12O19. Z Kristallogr. 1967;125:437–449.

[26] Obradors X, Solans X, Collomb A, Samaras D, Rodriguez J, Pernet M, et al. Crystal structure of strontium hexaferrite SrFe12O19. J Solid State Chem. 1988;72(2):218–224.

[27] Pullar RC, Bhattacharya AK. The synthesis and characterization of Co2X (Ba2Co2Fe28O46) and Co2U (Ba4Co2Fe36O60) ferrite fibres, manufactured from a sol–gel process. J Mater Sci. 2001;36(19):4805–4812.

[28] Shirk BT, Buessem WR. Temperature dependence of Ms and K1 of BaFe12O19 and SrFe12O19 single crystals. J Appl Phys. 1969;40(3):1294–1296.

[29] Evans BJ, Grandjean F, Lilot AP, Vogel RH, Gérard A. 57Fe hyperfine interaction parameters and selected magnetic properties of high purity MFe12O19 (M = Sr, Ba). J Magn Magn Mater. 1987;67(1):123–129.

[30] Le Breton JM, Teillet J, Wiesinger G, Morel A, Kools F, Tenaud P. Mössbauer

Online ISSN 3007-3197
Print ISSN 3007-3189
http://amresearchreview.com/index.php/Journal/about

investigation of Sr-Fe-O hexaferrites with La-Co addition. IEEE Trans Magn. 2002;38(5):2952–2954.

[31] Shirk BT, Buessem WR. Magnetic properties of barium ferrite formed by crystallization of a glass. J Am Ceram Soc. 1970;53(4):192–196.

[32] Arendt RH. The molten salt synthesis of single magnetic domain BaFe12O19 and SrFe12O19 crystals. J Solid State Chem. 1973;8(4):339–347.

[33] Ding J, Maurice D, Miao WF, McCormick PG, Street R. Hexaferrite magnetic materials prepared by mechanical alloying. J Magn Magn Mater. 1995;150(3):417–420.

[34] Luo H, Rai BK, Mishra SR, Nguyen VV, Liu JP. Physical and magnetic properties of highly aluminum doped strontium ferrite nanoparticles prepared by auto-combustion route. J Magn Magn Mater. 2012;324(17):2602–2608.

[35] Pechini MP. Method of preparing lead and alkaline earth titanates and niobates and coating method using the same to form a capacitor. US Patent 3,330,697. 1967.

[36] Saura-Múzquiz M, Eikeland AZ, Stingaciu M, Andersen HL, Avdeev M, Christensen M. Synthesis, crystal structure, site occupancy, and magnetic properties of aluminum-substituted M-type Sr hexaferrite SrFe12−xAlxO19 nanoparticles. Chem Mater. 2025. doi:10.1021/acs.chemmater.4c02205.

[37] Makovec D, Primc D, Šturm S, Kodre A, Hanžel D, Drofenik M. Structural properties of ultrafine Ba-hexaferrite nanoparticles. J Solid State Chem. 2012;196:63–71.

[38] Drofenik M, Ban I, Makovec D, Žnidaršič A, Jagličić Z, Hanžel D, et al. The hydrothermal synthesis of super-paramagnetic barium hexaferrite particles. Mater Chem Phys. 2011;127(3):415–419.

[39] Pullar RC, Taylor MD, Bhattacharya AK. A halide free route to the manufacture of microstructurally improved M ferrite (BaFe12O19 and SrFe12O19) fibres. J Eur Ceram Soc. 2002;22(12):2039–2045.

[40] Morel A, Le Breton JM, Kreisel J, Wiesinger G, Kools F, Tenaud P. Sublattice occupation in Sr1−xLaxFe12−xCoxO19 hexagonal ferrite analyzed by Mössbauer spectrometry and Raman spectroscopy. J Magn Magn Mater. 2002;242–245:1405–1407.

[41] Asti G, Bolzoni F, Le Breton JM, Ghidini M, Morel A, Solzi M, et al. Magnetic anisotropy of LaCo-substituted SrFe12O19 ferrites. J Magn Magn Mater. 2004;272–276:E1845–E1846.

[42] Rietveld HM. A profile refinement method for nuclear and magnetic structures. J Appl Crystallogr. 1969;2(2):65–71.

[43] Patterson AL. The Scherrer formula for X-ray particle size determination. Phys Rev. 1939;56(10):978–982.

[44] Williamson GK, Hall WH. X-ray line broadening from filed aluminium and wolfram. Acta Metall. 1953;1(1):22–31.

[45] Waldron RD. Infrared spectra of ferrites. Phys Rev. 1955;99(6):1727–1735.

[46] Kreisel J, Lucazeau G, Vincent H. Raman spectra and vibrational analysis of BaFe12O19 hexagonal ferrite. J Solid State Chem. 1998;137(1):127–137.

[47] Meshram MR, Agrawal NK, Sinha B, Misra PS. Characterization of M-type

Online ISSN 3007-3197
Print ISSN 3007-3189

barium hexagonal ferrite-based wide band microwave absorber. J Magn Magn Mater. 2004;271(2–3):207–214.

[48] Stoner EC, Wohlfarth EP. A mechanism of magnetic hysteresis in heterogeneous alloys. Philos Trans R Soc Lond A. 1948;240(826):599–642.

[49] Ishiwata S, Taguchi Y, Murakawa H, Onose Y, Tokura Y. Low-magnetic-field control of electric polarization vector in a helimagnet. Science. 2008;319(5870):1643–1646.

[50] Chun SH, Chai YS, Jeon BG, Kim HJ, Oh YS, Kim I, et al. Electric field control of nonvolatile four-state magnetization at room temperature. Phys Rev Lett. 2012;108(17):177201.

[51] Harris VG, Chen Z, Chen Y, Yoon S, Sakai T, Geiler A, et al. Ba-hexaferrite films for next generation microwave devices. J Appl Phys. 2006;99(8):08M911.

[52] Wang J, Yang A, Chen Y, et al. Self-biased Y-junction circulator at Ku band. IEEE Microw Wirel Compon Lett. 2011;21(6):292–294.

[53] Coey JMD. Magnetism and Magnetic Materials. Cambridge: Cambridge University Press; 2010.

[54] Ong SP, Richards WD, Jain A, Hautier G, Kocher M, Cholia S, et al. Python Materials Genomics (pymatgen): a robust, open-source python library for materials analysis. Comput Mater Sci. 2013;68:314–319.

[55] Kittel C. Theory of the structure of ferromagnetic domains in films and small particles. Phys Rev. 1946;70(11–12):965–971.

[56] Namai A, Yoshikiyo M, Yamada K, Sakurai S, Goto T, Yoshida T, et al. Hard magnetic ferrite with a gigantic coercivity and high frequency millimetre wave rotation. Nat Commun. 2012;3:1035.

[57] Sleptsova AE, Alyabyeva LN, Gorbachev EA, Kozlyakova ES, et al. Tuning the morphology and magnetic properties of single-domain SrFe8Al4O19 particles prepared by citrate auto-combustion route. arXiv:2101.03993 [Preprint]. 2021.

[58] Coey JMD. Permanent magnets: plugging the gap. Scr Mater. 2012;67(6):524–529